ATION PAGE

Form Approved
OMB No 0704-0188

(2)

1. AGENCY USE ONLY	2. REPORT DATE	3. REPORT TYPE AND DATES COVERED
	October 29, 1992	Final Tech (July 1, 1989-October 31,1992

4. TITLE AND SUBTITLE

Growth Studies of CVD-MBE by in-situ diagnostics

5. FUNDING NUMBERS

G-N00014-89-J-3120

6. AUTHOR(S)

Dr. George N. Maracas
Dr. Timothy C. Steimle

7. PERFORMING ORGANIZATION NAME(S) AND ADDRESS(ES)

Arizona State University
College of Engineering and Applied Sciences
Department of Electrical & Computer Engineering
Tempe, AZ 85287-5706

8. PERFORMING ORGANIZATION REPORT NUMBER

DWA 1757

9. SPONSORING / MONITORING AGENCY NAME(S) AND ADDRESS(ES)

DARPA Defense Sciences Office
1400 Wilson Blvd.
Arlington, VA 22209-2308

Administered by....
Office of Naval Research-Resident Representative
University of New Mexico
Bandelier Hall West, Room 111
Albuquerque, NM 87131-0001

10. SPONSORING / MONITORING AGENCY REPORT NUMBER

11. SUPPLEMENTARY NOTES

12a. DISTRIBUTION / AVAILABILITY STATEMENT

Available to the public

12b. DISTRIBUTION CODE

13. ABSTRACT *(Maximum 200 words)*

This is the final technical report for the three year DARPA - URI program "Growth Studies of CVD-MBE by in-situ Diagnostics." The goals of the program were to develop non-invasive, real time epitaxial growth monitoring techniques and combine them to gain an understanding of processes that occur during MBE growth from gas sources. We have adapted these techniques to a commercially designed gas source MBE system (Vacuum Generators Inc.) to facilitate technology transfer out of the laboratory into industrial environments.

The in-situ measurement techniques of spectroscopic ellipsometry (SE) and laser induced fluorescence (LIF) have been successfully implemented to monitor the optical and chemical properties of the growing epitaxial film and the gas phase reactants. The ellipsometer was jointly developed with the J. Woolam Co. and has become a commercial product.

The temperature dependence of group III and V desorption from GaAs and InP has been measured as well as the incident effusion cell fluxes. The temporal evolution of the growth has also been measured both by SE and LIF to show the smoothing of heterojunction surfaces during growth interruption. Complicated microcavity optical device structures have been monitored by ellipsometry in real time to improve device quality. This data has been coupled with the structural information obtained from reflection high energy electron diffraction (RHEED) to understand the growth processes in binary and ternary bulk III-V semiconductors and heterojunctions. Using these techniques we have attained record narrow photoluminescence (PL) linewidths in quantum wells as well as record on/off ratio asymmetric Fabry Perot reflection modulators.

The tools developed under this DARPA program have thus set the basis for future work in advanced sensors and intelligent processing.

14. SUBJECT TERMS	15. NUMBER OF PAGES
Semiconductor growth - MBE	37
	16. PRICE CODE

17. SECURITY CLASSIFICATION OF REPORT	18. SECURITY CLASSIFICATION OF THIS PAGE	19. SECURITY CLASSIFICATION OF ABSTRACT	20. LIMITATION OF ABSTRACT
UNCLASSIFIED	UNCLASSIFIED	UNCLASSIFIED	

(12)

Final Technical Report

July, 1 1989 - June 30, 1992

Growth Studies of CVD-MBE by In-situ Diagnostics

George N. Maracas
Timothy C. Steimle

Arizona State University
Tempe, AZ 85287-5706

Sponsored
by
Defense Advanced Research Projects Agency
University Research Initiative (URI)

and

Office of Naval Research

Contract number N00014-89-J-3120

Abstract

This is the final technical report for the three year DARPA - URI program "Growth Studies of CVD-MBE by in-situ Diagnostics." The goals of the program were to develop non-invasive, real time epitaxial growth monitoring techniques and combine them to gain an understanding of processes that occur during MBE growth from gas sources. We have adapted these techniques to a commercially designed gas source MBE system (Vacuum Generators Inc.) to facilitate technology transfer out of the laboratory into industrial environments.

The in-situ measurement techniques of spectroscopic ellipsometry (SE) and laser induced fluorescence (LIF) have been successfully implemented to monitor the optical and chemical properties of the growing epitaxial film and the gas phase reactants. The ellipsometer was jointly developed with the J. Woolam Co. and has become a commercial product.

The temperature dependence of group III and V desorption from GaAs and InP has been measured as well as the incident effusion cell fluxes. The temporal evolution of the growth has also been measured both by SE and LIF to show the smoothing of heterojunction surfaces during growth interruption. Complicated microcavity optical device structures have been monitored by ellipsometry in real time to improve device quality. This data has been coupled with the structural information obtained from reflection high energy electron diffraction (RHEED) to understand the growth processes in binary and ternary bulk III-V semiconductors and heterojunctions. Using these techniques we have attained record narrow photoluminescence (PL) linewidths in quantum wells as well as record on/off ratio asymmetric Fabry Perot reflection modulators.

The tools developed under this DARPA program have thus set the basis for future work in advanced sensors and intelligent processing.

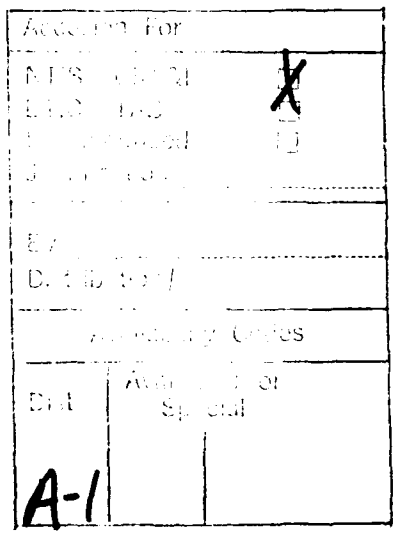

Table of Contents

1. Introduction

During the first year of the DARPA-URI program, effort was directed almost exclusively toward hardware and software development of in-situ MBE growth monitoring techniques and hydride cracker design. We have successfully redesigned our hydride cracker [1] for improved cracking efficiency and flux uniformity. A number of prototype systems were constructed for spectroscopic ellipsometry (SE) and laser induced fluorescence (LIF) which had the capability of being adapted to a commercial MBE system. A collaboration with the J.A. Woolam Co. (who is a DARPA contractor) in spectroscopic ellipsometry was established and resulted in the present SE system. The goals of this time period were to obtain a capability with which the growth of semiconductor surfaces could be monitored by three complementary techniques having submonolayer sensitivity and time resolution on the order of constituent surface migration times. We have been successful in these goals and have achieved a unique facility with which to monitor optical, chemical and structural properties of the growing surface in an MBE having gaseous sources.

In the second year we continued to identify technical aspects of in-situ characterization specific to the growth monitoring application and have refined our systems to the point where we have measured several important growth parameters. Our concentration, however, was to use the techniques to obtain relevant parameters for use in growth models. This progress is described in the body of this report.

During the third year we used the in-situ tools that we developed to monitor technologically important epitaxial structures such as semiconductor quantum wells and microcavity optical devices (vertical cavity lasers and spatial light modulators). We also obtained the first high temperature optical constants of AlAs and AlGaAs and used the data to calibrate thickness and composition at the growth temperature. This aspect of the research has enabled us to drastically reduce the calibration time required for complicated epitaxial structure growth. We also observed for the first time a difference in the desorption activation energy of indium from surfaces of having different reconstructions.

The progress under this research program has led to several major developments. The developments are in the areas of in-situ measurement development and implementation, improved growth resulting from the information gleaned from the data and measurement of properties not possible before. The main points are itemized here and discussed in subsequent sections.

We have:

* developed an in-situ spectroscopic ellipsometry system in conjunction with the J.A. Woolam Co. that is compatible with both MBE and MOCVD reactors. The prototypes resulting from the joint collaboration have resulted in a commercial product that is the most flexible and advanced available to date. As of the present time, approximately 20 have been sold worldwide.
* identified and addressed problems with adapting in-situ optical measurements on commercial MBE systems. Design criteria have been relayed to MBE manufacturers for commercial system modification. Such modifications are now either options or standard from the manufacturers.
* designed and tested a high efficiency, high uniformity group V hydride cracking cell for gas source MBE.
* used SE to measure the MBE substrate temperature from room temperature to typical growth temperatures. This is a major extension over conventional measurement techniques (optical pyrometry) which accurately determine temperature only above 400°C.
* been the first to track the growth of an MBE multiple quantum well by SE.
* measured the interfacial layer roughness at the inverted" GaAs on AlAs interface and compared it to the "normal" AlAs on GaAs interface.

* constructed a laser induced fluorescence system and adapted it to a commercial MBE system for monitoring of MBE growth processes. Atomic group III and dimeric As_2 and P_2 have been identified and characterized.
* quantified the thermal desorption properties of indium and P_2 on InP substrates by LIF.
* measured desorption activation energies of In versus GaAs surface reconstruction and compared with those obtained on InP.
* used the techniques developed to grow GaAs/AlGaAs quantum wells in GSMBE with record narrow luminescence linewidths of 0.6 meV at 2K for a 100Å well.
* been the first to adapt spectroscopic ellipsometry to the growth of AlGaAs based microcavity optical devices. This has helped realize reflection asymmetric Fabry Perot electro-optic modulators with record high on/off ratio of 1200.

2. Spectroscopic ellipsometry

Spectroscopic ellipsometry (SE) is based on measuring the polarization state of reflected light, at multiple wavelengths, when linearly polarized light is made incident on a sample. This is achieved by determining a complex reflection coefficient ratio ρ of the sample, which in turn is defined as the quotient of the complex reflection coefficients for light polarized parallel (R_p) and perpendicular (R_s) to the plane of incidence. In the simplest case of the two-phase model which consists of ambient (air or vacuum) / substrate with no additional layers, $R_{p,\,s}$ represent the Fresnel reflection coefficients of the system. Usually, ρ is transformed into the "ellipsometric parameters" Ψ and Δ, which characterize the polarization state of the reflected light according to the relation:

$$\rho = \frac{R_p}{R_s} = \tan(\Psi)e^{i\Delta}, \qquad (1)$$

where $\tan(\Psi)$ is the amplitude and Δ is the phase difference between the two components of the electric field. The SE experimental measurements are expressed as $\Psi(h\nu_i, \Phi_j)$ and $\Delta(h\nu_i, \Phi_j)$ where $h\nu_i$ is the photon energy and Φ_j is the external angle of incidence. Measurements in an MBE growth chamber [2-5] are most often performed at a fixed angle of incidence because of the fixed optical port geometry. The measured ellipsometric parameters, Ψ and Δ, are sensitive to the structure (layer thicknesses, compositions, microstructure, etc.) and the optical constants of the sample. In addition, SE is sensitive to any physical property or process which affects the optical constants and/or surface or interface conditions: i.e. for example temperature.

To extract surface temperature by SE, it is necessary to known a priori the temperature dependent optical constants [6,7] for the particular material studied. The range in which the temperature can be measured is limited to the range over which the optical constants are known. The determination of temperature dependent optical constants for GaAs has only recently been achieved by Yao, Snyder, and Woollam [3]. These pseudo-optical constants [3] of GaAs serve as a set of reference functions, which we have used to find unknown sample surface temperatures by fitting the measured data.

The concept of using ellipsometry to measure the surface temperature of a Si substrate in a UHV setting was first suggested by Ibrahim and Bashara in 1972 [8]. Tomita et al [9], in 1986, also proposed the use of ellipsometry to measure the surface temperature of Si and GaAs. We have successfully implemented this on our MBE system. We have found [10] (see figure 1) that the surface temperature in MBE can differ by more than 150°C from that measured by the thermocouple. Furthermore, using SE, we have extended the

temperature measurement range down to room temperature from the optical pyrometer limit of approximately 450°C. The measurement of surface temperature is extremely important in surface growth kinetics studies because of the inherently exponential temperature dependence of the reactions. With this technique, much of the ambiguity in interpreting sticking coefficients arising from errors in temperature measurement can be significantly reduced.

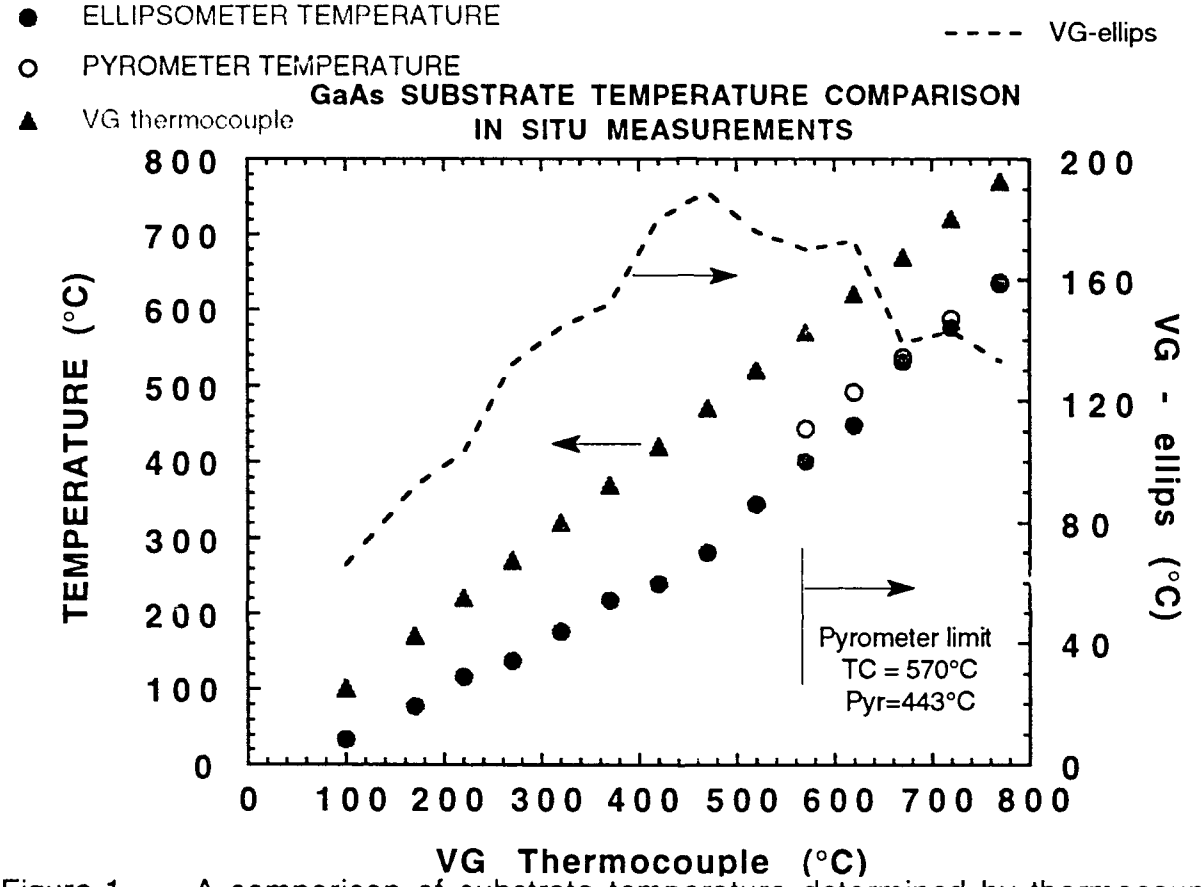

Figure 1 A comparison of substrate temperature determined by thermocouple, optical pyrometer and spectroscopic ellipsometer. The difference between the thermocouple and ellipsometer is plotted on the axis to the right. It should be noted that the ellipsometer can measure temperatures from typical growth temperatures to room temperature.

2.1. Optical constants of AlAs versus temperature

Ultimately the success of an in situ diagnostic tool is its applicability to monitor processes occurring under actual operating conditions (temperature, pressure, appropriate time scales, etc.). For III-V semiconductor epitaxial growth, this requirement is that alloy composition and thickness be measurable at the growth temperature (400°C - 700°C). There is a noticeable lack of high temperature optical constant data in the literature which has compelled us to obtain such constants for GaAs and AlAs. Previous optical constant temperature ranges [11,12] have been limited to below temperatures where group V surface desorption roughens the surface and makes ellipsometric analysis ambiguous.

Because MBE has the capability of producing high group V surface overpressures, a stoichiometrically intact (smooth) surface can be maintained to high temperatures. We have used this advantage to measure the optical constants of AlAs up to approximately 700°C. The temperature dependent optical constants will be published elsewhere [9].

The structure used to measure the optical constants was 10,000Å of AlAs grown on a semi-insulating GaAs substrate without a GaAs or As cap layer. The temperature of the GaAs substrate was calibrated with the ellipsometer and an optical pyrometer as discussed previously. The angle of incidence (75.2°) was also determined by SE to reduce errors due to angular uncertainties. Ellipsometric scans were fit to the structure using optical constants, n and k as independent fitting parameters. Optical constants were extracted at room temperature and 400°C to 700°C in 25°C increments after allowing sufficient time for the substrate temperature to stabilize.

Knowledge of the high temperature AlAs optical constants has enabled the thickness and alloy composition extraction of structures presented in this paper at the growth temperature of 623°C.

2.2. Dynamic growth rate modeling

One important parameter in epitaxial layer growth is the growth rate. Reflection high energy electron diffraction (RHEED) is typically used because one cycle of intensity oscillations corresponds to the growth of one atomic layer of material. Three problems with this surface-sensitive technique are that it cannot be used with substrate rotation, the oscillation intensity decays after the growth of tens of monolayers and oscillations occur only in layer-by-layer growth mode. SE, in comparison, can be performed under substrate rotation. Depending on the incident optical energy used in SE (typically 1-4eV), the light can sample both the surface and the entire volume of the epitaxial layer as opposed to RHEED (with energies of 5-20keV) which has a sampling depth (electron penetration depth) of a few angstroms. For this same reason SE data can be taken in either layer-by-layer or island growth mode.

If the optical constants at the growth temperature are known, then measurement of ellipsometric parameters can be made and thickness and alloy composition can be extracted as a function of time (dynamically) during the growth. We find that after an initial spectroscopic scan, only three wavelengths are required to obtain a reasonable accuracy in growth rate determination. Typically data is taken at a rate of 3.3 seconds per wavelength.

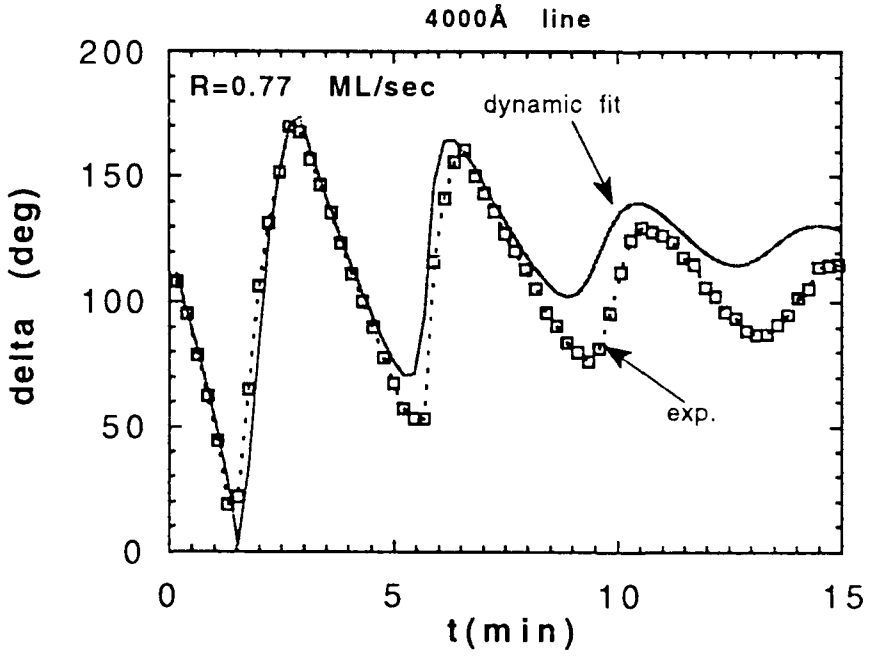

Figure 2 Dynamic fitting of Δ versus time during the growth of AlAs. The growth rate of 0.77 ML/s was extracted by the dynamic fit over approximately 15 minutes of data.

In an AlAs test structure the SE determined growth rate of 0.77 ML/sec agrees within 10% with the 0.83 ML/sec measured using the RHEED intensity oscillation technique. This discrepancy occurs because the growth rate on thick structures can decrease with effusion cell cooling while the shutter is open. Since SE measures the entire structure, it measures a growth rate averaged over any effusion cell flux temporal variations and thus can yield lower growth rates than RHEED. This is illustrated more completely in the DBR growth section.

Another consideration for studying epitaxial growth kinetics is the condition of the surface that is to be grown on. Often RHEED does not provide information on surface porosity (for example). Illustrated in figure 2 is a real-time ellipsometric trace of a typical growth run consisting of GaAs oxide desorption, substrate annealing, surface smoothing by a Ga pulse, the growth of 2000Å of $Al_{0.25}Ga_{0.75}As$ and a 500Å GaAs cap. The substrate is ramped to the appropriate temperatures required for growth of each layer. A gradual change of the optical properties of the native oxide is observed before the catastrophic "blow-off" is observed by RHEED. Aspnes [14] assumed a surface roughening model to describe such an effect. It is likely that a combination of surface roughening and a change of oxide composition (or optical constants) is occurring. We would like to obtain an independent measure of the change in oxide chemistry to confirm this hypothesis. No change is observed by RHEED during the anneal stage but a slight change is seen by SE. It should be noted that surface changes are observed even at the relatively long wavelength of 5000Å. As the wavelength is decreased, the measurement becomes more surface sensitive and, in fact, monolayer changes in surface have been observed [15] by our group. An example of this is shown in figure 3 which plots psi at 3000Å versus time after the Ga smoothing pulse indicated in figure 2. An exponential fit to the data is also shown indicating that after the Ga pulse occurs the surface stabilizes with a time constant of approximately 80 seconds at this substrate

temperature.

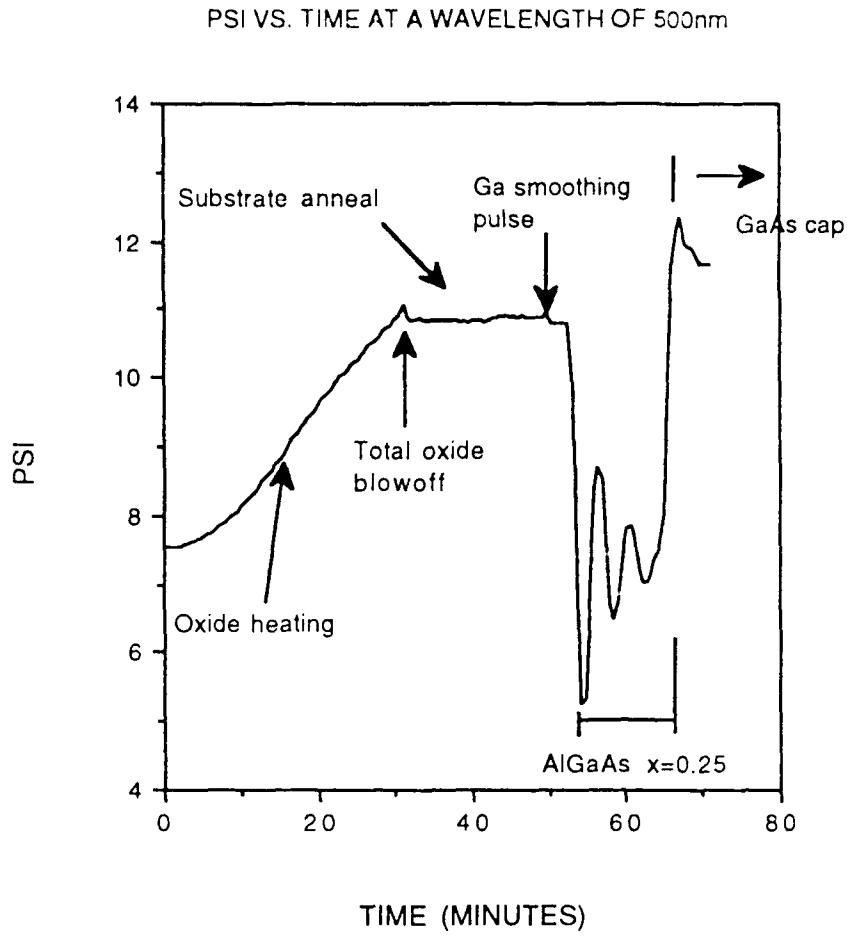

Figure 3 Real-time monitoring by of the growth of a thick (2500Å) AlGaAs epitaxial layer on a GaAs substrate. This curve was taken at a wavelength of 5000Å.

The corresponding Ψ versus Δ, or velocity plot, of this growth run is shown in figure 4. The trajectory converges to three main points corresponding to the optical constants of the optically thick native oxide, GaAs and AlGaAs. When the real and imaginary parts of the dielectric constant are plotted as in figure 4, the position of the locus is an indication of the alloy composition of the epitaxial layer. Aspnes [14] has used this to control aluminum composition in a CBE system. Consequently, the alloy composition of the film can be determined during growth and also after growth is terminated. Each point represents a multiple wavelength spectroscopic scan. For fast surface processes, a scan at a single wavelength can be performed which can resolve features occurring in the several hundred millisecond time scale.

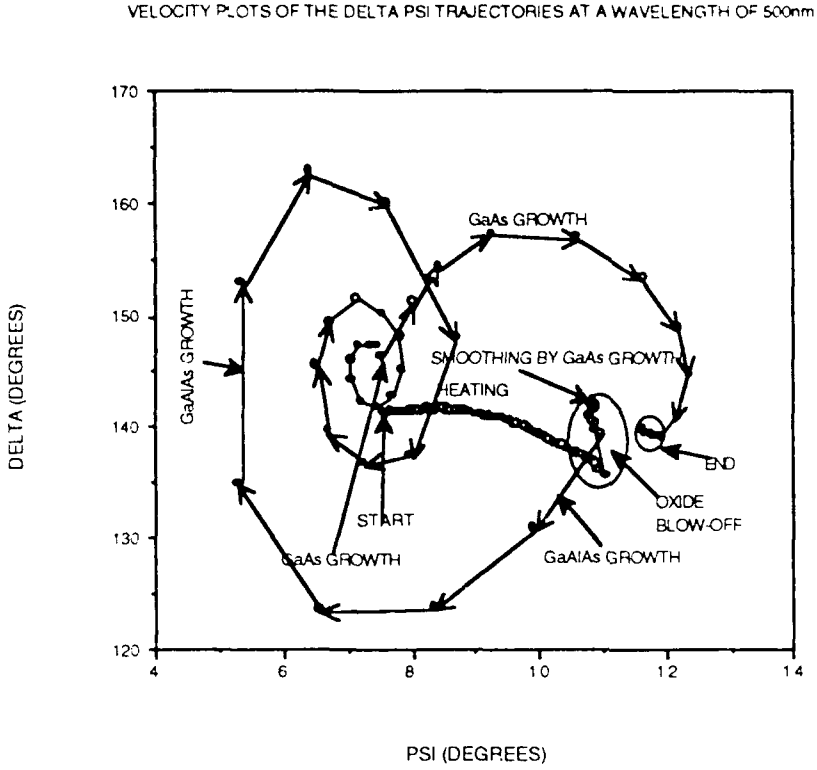

Figure 4 The velocity plot corresponding to the growth run shown in figure 2 shows the spiraling of the trajectory to the optically thick values of GaAs and AlGaAs at the wavelength of 5000Å.

2.3. Quantum well growth

Quantum devices require thickness and heterojunction abruptness control on the order of one monolayer (ML) to produce narrow energy optical transitions that occur at the designed energy. We were able to observe the QW thickness and interface properties using SE during the growth cycle.

Two single quantum well structures were grown consecutively under identical growth conditions except that one had a 60 second growth interruption at the bottom GaAs on AlAs "inverted" interface. These will be called sample I (with interruption) and NI (no interruption) for convenience. The "inverted" interface has been found to produce poor electrical properties in high electron mobility transistors because of impurity incorporation and roughness caused by alloy intermixing at the interface. This effect is also responsible in some cases for broad luminescence transition linewidths.

Two test samples were grown consisting of a 1000Å GaAs buffer layer, followed by a 100Å AlAs barrier, a 70Å GaAs well, a 100Å AlAs barrier and finally a 20Å GaAs cap layer. Both structures were undoped, grown at 600°C with a 60 sec. growth interruption at the top AlAs/GaAs QW interface. One QW structure (NI) had no growth interruption at the bottom GaAs-on-AlAs interface and the other layer (I) had a 60 second interruption.

Figure 1 shows Ψ (at λ=3550Å) as a function of time during the growth of the two quantum wells with and without a 60 second interruption at the "inverted" interface. The wavelength of 3550Å was used for display purposes because it was more sensitive to near-surface phenomena due to its small absorption depth at this temperature. The sloped characteristics of the individual AlAs layers arise from the layers being optically thin at this wavelength. During the growth interruption time (labeled "int."), the slopes of the curves at this wavelength are approximately zero .

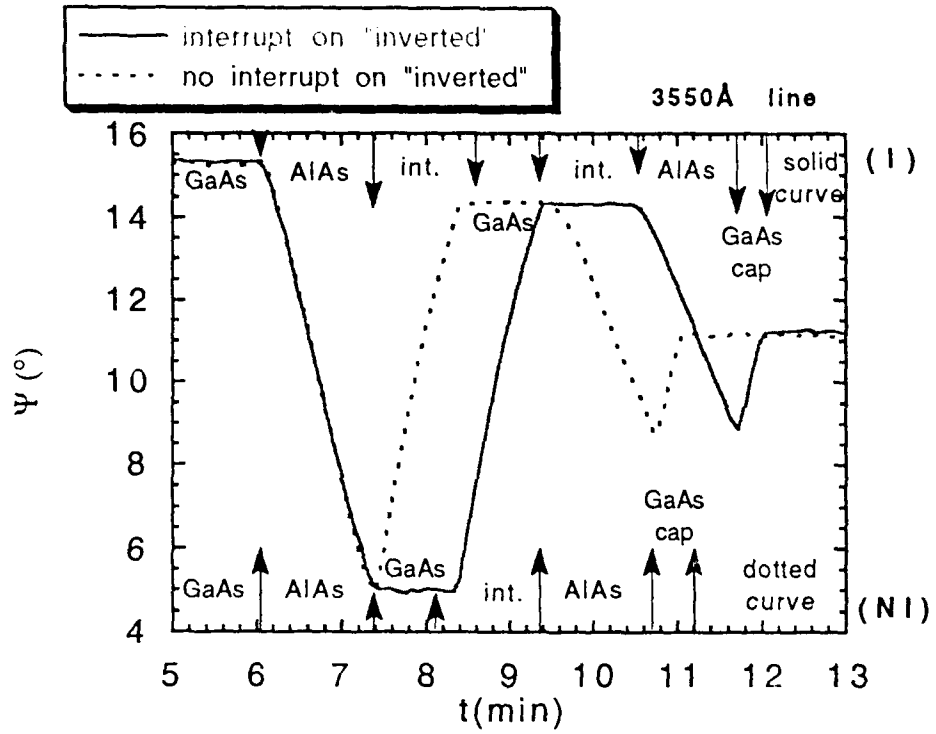

Figure 5. Tracking of two quantum well growth runs. One quantum well had a 60 second interruption at the "inverted" GaAs on AlAs surface while the other had none.

Fits to the ellipsometric spectra yielded a quantum well width of 70Å and barriers of 100Å indicating that the growth of the wells was successful.

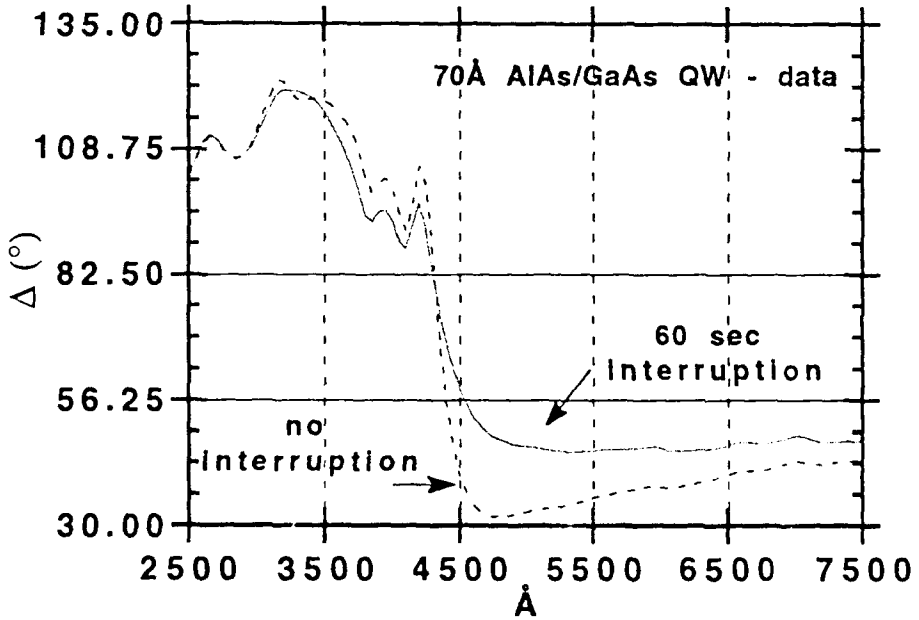

Figure 6 Raw data for SE scan of the two AlAs/GaAs quantum well structures (one with interruption and the other without growth interruption at the "inverted" interface).

Independent photoluminescence measurements confirmed the well thickness in both samples and showed a difference in the n=1 heavy hole transitions of less than 0.5 meV indicating high reproducibility of the growth process. Shoulders 4meV on either side of main

photoluminescence transition indicated that the quantum well grown without interruption (NI) had interface roughness on the order of ±1 monolayers. The measured shoulder energies agreed very well with solutions to Schrödinger's equation for quantum wells having ±1 ML differences in width. SE analysis [16] extracted an interfacial layer thickness in the quantum well of 1.4ML which agrees with the photoluminescence.

Thus it is demonstrated that SE can have thickness sensitivity on the order of a monolayer and can be used to monitor the width of a quantum well during the growth process. This information allows the grower to control the thickness by adjusting the growth rate and/or time for each layer without requiring removal from the MBE for ex-situ material structure evaluation.

2.4. Bragg reflectors

Dielectric mirrors require layer thickness uniformity among successive periods to produce high reflectance in a given wavelength range. This uniformity is a result of interface flatness and a random or systematic variation thickness in successive layers. Interface roughness degrades the peak reflectance [17] while systematic and random thickness variations skew and increase the side lobe reflectance respectively. Our calculations show that the thickness deviation required to maintain near peak reflectance in a DBR stack is less than 8% for a 20 period DBR. The design of a mirror presented here with stop band centered at 867nm consists of AlAs/$Al_{0.2}$GaAs quarter wavelength layers of thicknesses 728Å and 628Å respectively. Thus a maximum 8% variation imposes the requirement that the optical thickness (= layer thickness/index of refraction) variation among the layers be less than 58Å and 50Å respectively. This tolerance must be maintained over a relatively thick (2.7μm) 20 period mirror with control over both epitaxial layer thickness and alloy composition. The problem is increased in a vertical cavity structure where two Bragg reflectors must be stacked with an intermediate quantum well gain region. An in situ monitoring and control technique such as SE is thus desirable for such complicated structures.

A growth temperature of 623°C measured by optical pyrometer or 616°C by SE (750°C as measured by the MBE thermocouple) was used to grow the 20 period DBR with thicknesses mentioned previously centered at 867nm. To reduce interface roughness, the $Al_{0.2}Ga_{0.8}As$ quarter wave layers were approximated by a GaAs and $Al_{0.3}Ga_{0.7}As$ superlattice. The mirror was grown on a 3300Å n^+ GaAs buffer on an n^+ substrate.

The AlAs optical constants [13] for the growth temperature were used to fit the ellipsometric data for thickness and alloy composition. Before growth, a full spectroscopic scan (200 - 770nm) was performed on the GaAs substrate to measure the temperature. Ψ and Δ were then measured at three wavelengths; 3500Å, 5500Å and 6500Å at a rate of one point (three wavelengths) every three seconds. Full spectroscopic scans were performed after the growth of periods 1, 2-5, 6-10, 11-15 and 16-20 to illustrate the thickness variation among successive layers and to monitor the evolution of the mirror reflectance. The growth rate was calibrated by SE after the growth of period 1. Figure 2 is a plot of the Ψ(t, 3500Å) data with the aforementioned intervals superimposed.

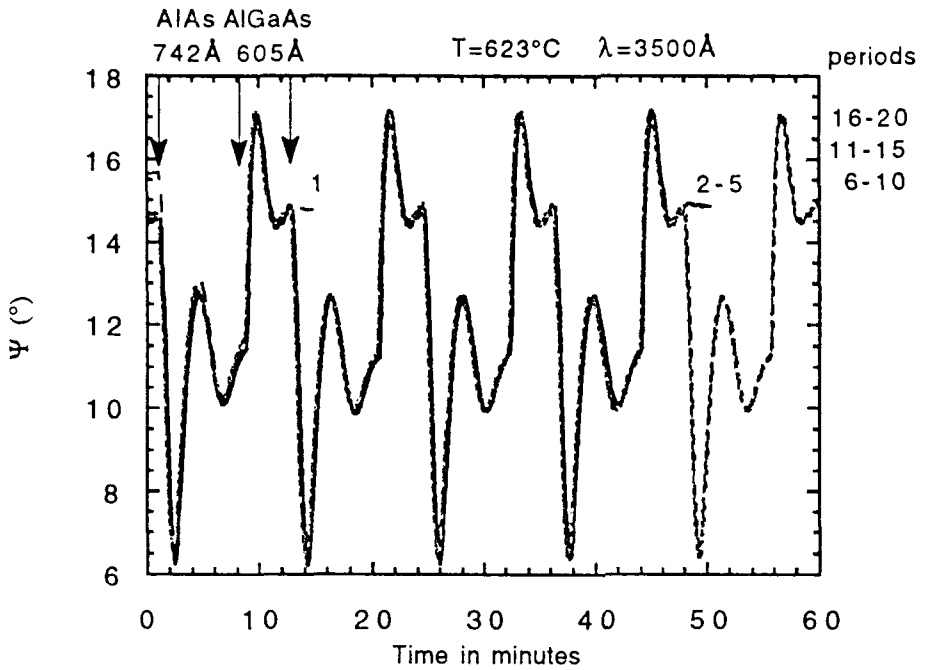

Figure 7. Dynamic growth monitoring of a 20 period AlAs/AlGaAs distributed Bragg reflector in the MBE at the growth temperature of 623°C. The periodicity of the mirror is evident in Ψ as a function of time. Superimposed are the curves of periods 1, 2-5, 6-10, 11-15 and 16-20 identified when the periods end. The time axis has been shifted such that successive period scans begin at t=0. A high degree of thickness and alloy composition reproducibility is evident from the superimposed curves.

While Ψ and Δ for all three wavelengths were used in the structural calculations, only Ψ is plotted for illustrative purposes. The time axes on the successive mirror portions were shifted such that each portion began at t=0. The numbers in figure 2 indicate the times where the data for each portion ended and the arrows denote the AlAs and $Al_{0.2}Ga_{0.8}As$ superlattice (SL) layers. The reproducibility of Ψ in subsequently grown layers shows that there is a high degree of optical thickness uniformity among all the periods of the DBR indicating a high effusion cell flux stability. The thickness and growth rate were calculated dynamically during the growth and compared well with the RHEED oscillations. RHEED measured growth rates of 97.6Å/min and 154.4Å/min for AlAs and the $Al_{0.2}Ga_{0.8}As$ SL layers respectively while SE measured 95.3Å/min and 156.8Å/min for AlAs and the $Al_{0.2}Ga_{0.8}As$ SL layers respectively. An effective medium approximation was used for analyzing the superlattice regions. This assumption of a uniform average alloy composition for the superlattice proved to be sufficiently accurate for this application.

Figure 3 shows SE scans after the growth of the various mirror portions with the substrate scan included for reference.

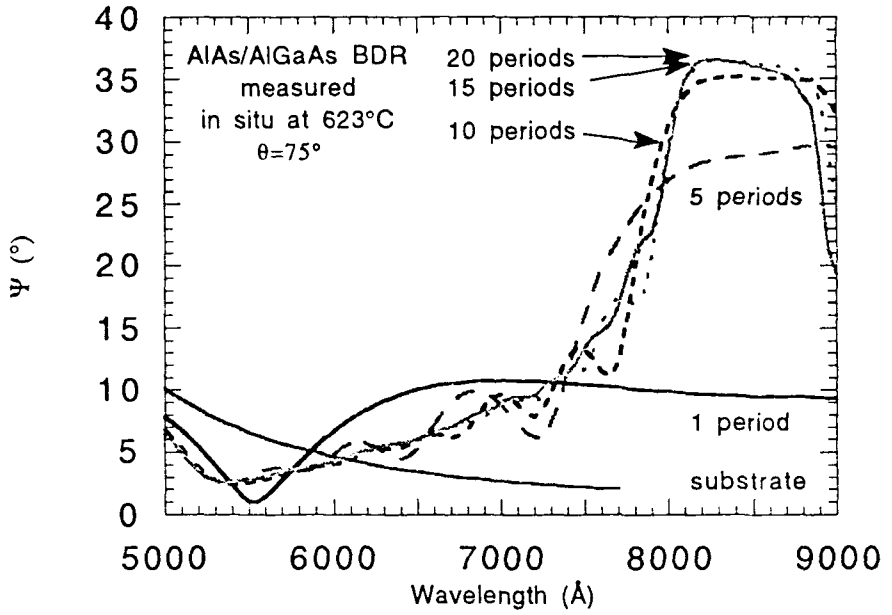

Figure 8. Measurement of Ψ versus wavelength of a distributed Bragg reflector at the growth temperature of 623°C in the MBE. The spectra were taken before the epitaxial structure was grown and after the growth of 1, 5, 10, 15 and 20 periods of the mirror. The angle of incidence of the incident light was 75°.

Ψ is plotted since it is the ratio of the amplitude change upon reflection (eq. 1) and thus is more closely related to the normal incidence reflectance than is Δ. It is interesting to note that the maximum value of Ψ saturates with increasing number of periods at approximately 15 as does the normal incidence reflectance. Evolution of the side lobes is also evident in the Ψ(λ) curves for periods greater than 5.

It should be recalled that Ψ and Δ are measured at oblique incidence (75°) and cannot be converted to an absolute, normal incidence reflectance using just a two layer model. The normal incidence reflectance can, however, be obtained from Ψ and Δ if the structural information (thicknesses and optical constants) is used and an analysis similar to the scattering matrix approach [18] performed. Shown in figure 4 is a comparison of the normal incidence reflectance and Ψ which was measured at 75°. This data was measured at room temperature outside of the MBE. The most notable feature is the shift in the stop band. This arises partly from the difference in the angle of incidence but also from nonuniformity in the group III flux making the position of the in situ measurement on the substrate different than that of the ex-situ measurement.

Normal incidence reflectance was measured against a standard reflector using a measurement system of our own design which alternates the reference and reflected beams onto one detector. Plotted in figure 5 is the calculation for the nominal design structure centered at 8670Å, the calculation for a mirror using the ellipsometrically determined thicknesses and compositions (at the growth temperature of 623°C) and the measured reflectance of the DBR discussed in this section.

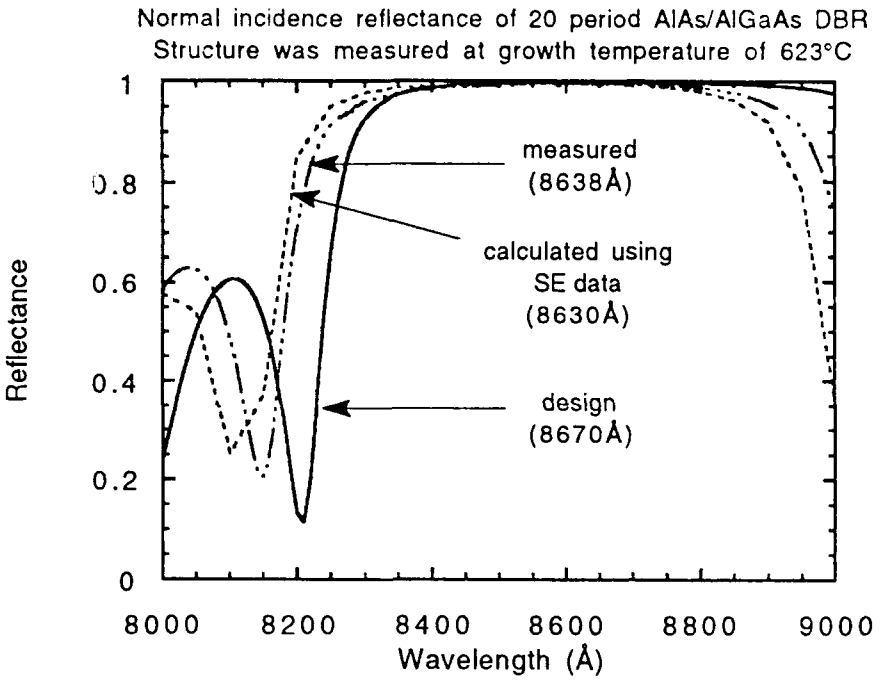

Figure 9. Normal incidence reflectance of a 20 period AlAs/AlGaAs distributed Bragg reflector. The mirror was designed for λ=867nm. The as-grown structure parameters were measured by SE at 623°C. Measured and calculated reflectance curves for the mirror are shown.

Thicknesses of the AlGaAs (superlattice) and AlAs were 606.2Å and 742.5Å respectively and x=0.19 and 1.0 respectively as measured by SE at the growth temperature. The peak reflectance was measured to be 0.995±0.004 at λ=8638Å (32Å from the design value) as compared to the calculated 0.997 at 8630Å. This reflectivity is higher than any previously reported for a 20 period DBR.

In summary, it was shown that SE is a viable in situ monitoring technique for growth of III-V photonic devices. SE can be used to measure substrate temperature, growth rate, alloy composition, thickness and heterojunction interface properties. It can also be used to monitor the evolution of reflectivity and the stop band in distributed Bragg reflectors. Combination of all these aspects of SE with MBE can thus provide the material grower with information for control of complicated structures required to realize reproducible photonic device operating characteristics.

For the growth of quantum wells and superlattices a high degree of interface smoothness is required. Thus a non-invasive real-time monitor of the growth conditions required for interface smoothness [15] is essential. We have the capability to take approximately ten ellipsometric data points per second which, at a growth rate of one monolayer per second, can provide sufficient resolution to monitor this parameter. Proof of this is in figure 5 in which we show the growth of GaAs/AlGaAs multiple quantum wells. The wells are 100Å wide while the barriers are 200Å. We are in the process of explaining the observed behavior.

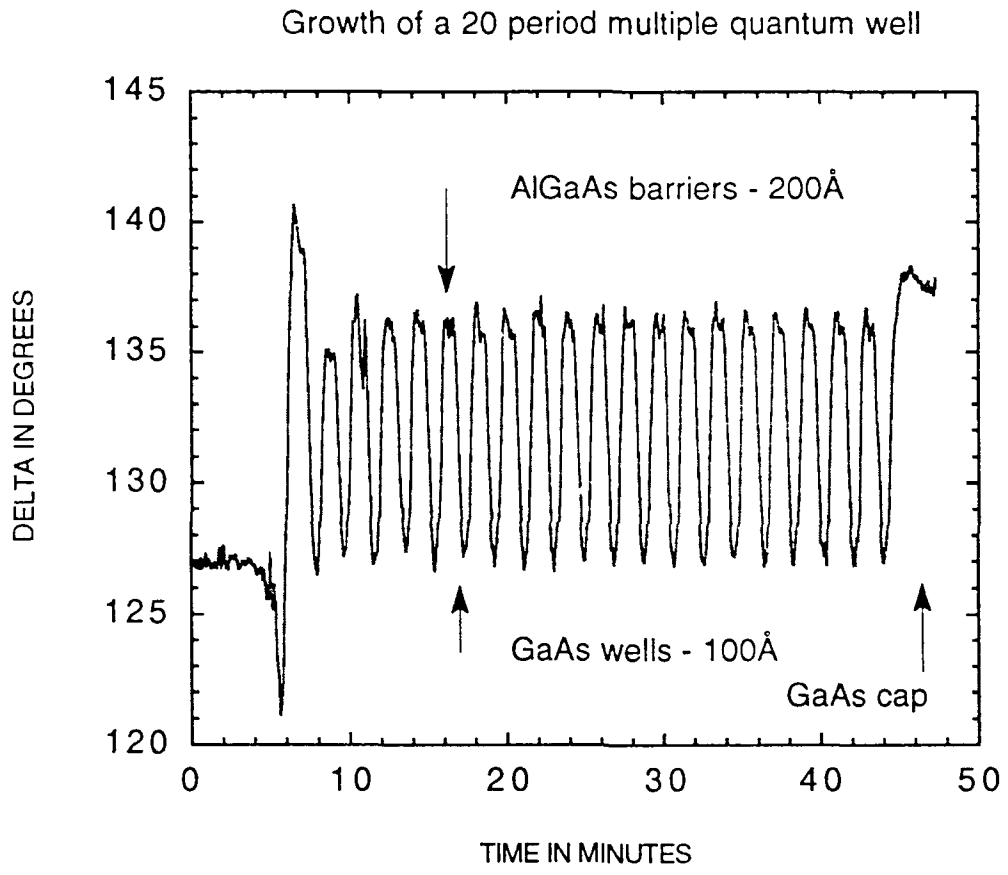

Figure 10 Ellipsometric tracking of the growth of a 20 period MBE AlGaAs/GaAs multiple quantum well.

In summary we have shown that in-situ ellipsometry can be used to study:

* changes in the semiconductor growth surface of approximately one monolayer
* the substrate surface temperature from room temperature to typical growth temperatures
* the evolution of growth in a multilayered structure
* interface roughness

These parameters are essential to complement the chemical and structural investigations and also to provide accurate values for growth models. In addition to the basic properties study, we have used the techniques described here to obtain record narrow photoluminescence linewidths [19] in GSMBE GaAs/AlGaAs quantum wells of 0.6 meV for a width of 100Å (see figure 6). Optimization of substrate temperature and growth interruption time were used to obtain these results. Figure 7 shows the best reported linewidths obtained with different growth techniques including ours.

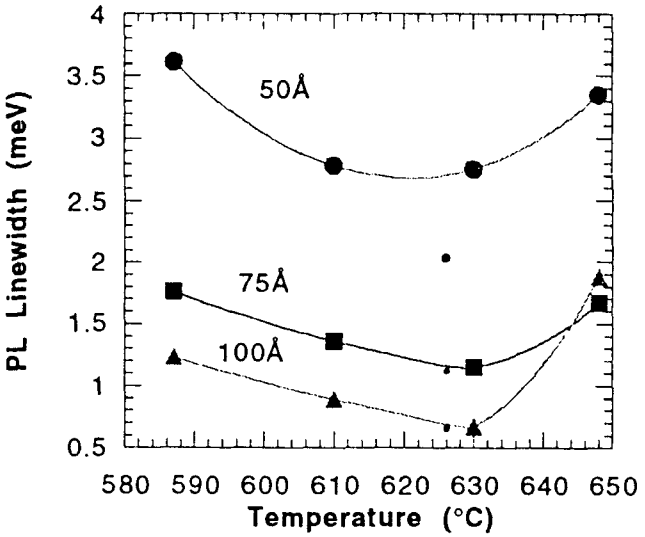

Figure 11 2K PL linewidths are plotted for 50Å, 75Å and 100Å GaAs/ AlGaAs QWs grown at different substrate temperatures. All QWs were grown with only one interrupt at the normal interface except for the QWs grown at 626°C which had interrupts both at the normal and inverted interfaces. The 2K PL linewidth for the 100Å GSMBE well is 0.62 meV which is the narrowest reported for GSMBE. The best linewidth obtained by solid source MBE was 0.5 meV but for a 175Å well.

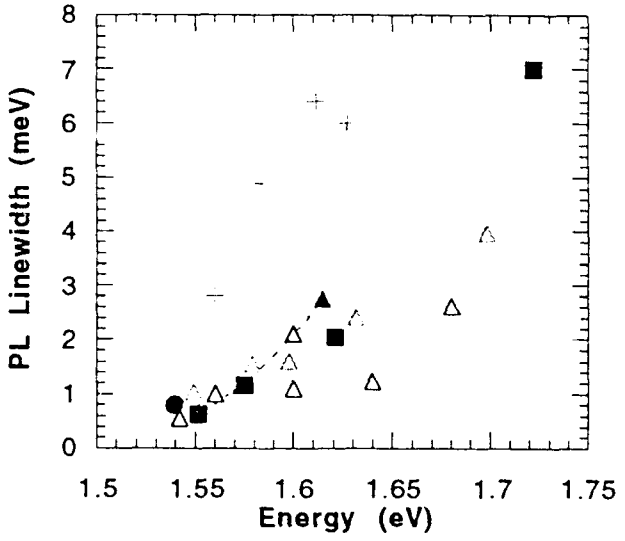

Figure 12 The reported best PL linewidths as a function of transition energies for single GaAs/ AlGaAs QWs of different width. Plotted are QWs grown by (●) MOCVD, (+) CBE, (Δ) MBE. Our data for GSMBE growth (■ -solid line) with interrupt at both interfaces and GSMBE (▲ -dotted line) with interrupt at only the normal interface are superimposed.

3. Reflection high energy electron diffraction

The RHEED technique has been developed to a high degree so that it is routinely used to measure the growth rate and the structural properties of the surface. RHEED is used most commonly to detect oxide desorption from the GaAs surface. It is also used to calibrate the temperature measurements by locating the transition position (congruent sublimation temperature) of the GaAs surface from arsenic stable (2x4) to a Ga stable (4x2). It is also used to study surface step distributions [20-22] by observing splitting of the diffraction streaks. In dynamic studies, the oscillations in the RHEED intensity of the specular beam during growth was found to correspond to the growth of monolayers.

Sustained RHEED oscillations during GaAs growth over long periods of time during GSMBE growth is a clear evidence of layer-by-layer growth during GSMBE. These oscillations, apart from being useful for the evaluation of growth rate and composition, are also useful in determining the effects of transients during shutter operation. These oscillations show very little change in growth rate even after growth of tens of monolayers. Transients are a strong function of crucible design and although the crucibles being used have terrible nonuniformity [24], they show a good transient response unlike the recent high uniformity cells that exhibit excellent uniformity characteristics but very poor transient response. A beat frequency associated with the oscillations is observed and this is a result of the growth non-uniformity as seen by the large RHEED spot in the absence of substrate rotation.

We have studied the recovery time of the RHEED intensity as a function of quantum well thickness [23]. Extensive studies at normal and inverted interfaces with and without growth interruption for QW growth have been performed and some of the results are mentioned here. We observed that there is no significant change in recovery time at the normal interface as a function of QW thickness. Even at growth rates of about 1μm per hour, complete recovery is seen within about 20 sec. This shows that an interrupt of 20 sec. at the normal interface provides adequate time for the completion of the monolayer and removal of excess Ga as suggested in the theory. As the growth temperature increases, the recovery becomes faster. This is due to the increased migration of atoms forming complete layers quickly. Below about 640°C, there is no significant change in oscillation period as a result of a constant growth rate.

A comparison of recovery of the RHEED intensity for growth with As_2 and As_4 at approximately 580°C has been performed. At low temperatures the intensity recovers quickly in the case of As_4, but never completely. Inability to recover to the original intensity indicates a small roughness which could be due to an incomplete layer that results with As_4 growth. However over long interrupt times, the intensity recovers to the initial value. In case of As_2, the recovery is complete and the intensity reaches the original starting intensity steadily, although the initial rise is slower as compared to As_4 growth. This result is attributed to the more efficient surface growth kinetics of As_2 and the contribution of hydrogen toward forming complete layers. The intensity at higher temperatures rises above the starting intensity. At higher temperatures the surface steadily gets rougher due to Ga desorption, resulting in a small decrease in intensity to begin with. However, immediately after growth, the surface is smooth again and longer interruption times at high temperatures slowly degrades the surface. Additional arsenic is needed to keep the surface stable above 640°C. During growth, the arsenic to gallium atom ratio is approximately 1.4. With As_4, this number is doubled since the incorporation efficiency is, at the best only 50%. The exact ratio of atoms is determined by arsenic induced oscillations. At the inverted interface, recovery time is affected by the percentage of aluminum present in the layers. At higher Al composition and at temperatures less than 620°C, the surface does not recover completely even after long interrupt times, indicating inability of Al atoms to migrate and form complete layers. The recovery of AlGaAs for composition of 0.3 that is commonly used, is very similar to the GaAs

surface. In contrast, AlAs growth shows a recovery of RHEED intensity at temperatures only above 660°C.

Molecular hydrogen was used to study its effects on GaAs growth in the cracker cell kept at 1000°C. No clear change in RHEED reconstructions were noticed even after extensive studies. Partial pressure of the added hydrogen was 1.5×10^{-5} mbar as measured from the BMIG. There is abundant hydrogen obtained from the cracking of arsine and hence the effect of additional hydrogen is relatively small. This however, was sufficient to cause a 4% decrease in growth rate as seen from the change in RHEED oscillations. Experiments with a gradual increase in hydrogen flow showed a corresponding decrease in growth rate. Hydrogen thus affects both Ga and As incorporation; but it has not been possible to obtain quantitative results. It is well known that in MBE, a surface above CST, in the absence of arsenic flux shows a Ga stable (4x2) reconstruction and below CST, an arsenic stable pattern is seen. However, in GSMBE, in the presence of residual hydrogen, even at temperatures as low as 580°C, the surface slowly turns to a Ga stable (1x3) or (4x2) in the absence of arsenic flux, indicating a slow removal process for arsenic covering the surface. At temperatures below 600°C, in the absence of hydrogen and arsenic, a Ga pre-deposited surface slowly changes from (4x2) to (2x4). In contrast, in GSMBE where there is a large quantity of residual hydrogen, the surface does not show any signs of change in reconstruction unless and until arsenic flux is turned on. These two observations, along with the reported GaAs etching results indicate a removal of arsenic and Ga atoms from the GaAs surface. Thus, hydrogen displaced arsenic is replaced by the arsenic over pressure and, free Ga is affected by hydrogen helps create an atomically sharp interface.

The observations justify the theoretically predicted model for growth kinetics with As_2 and hydrogen. The studies just mentioned enabled the determination of exact conditions for obtaining smooth interfaces with GSMBE growth.

Our recent studies include RHEED observations of InP growth on GaAs substrate. The initial island formation and the occurrence of 3D growth with the deposition of InP monolayers have been monitored. We have tracked the evolution of the RHEED patterns along the [1$\underline{1}$0] direction after 1, 4 and 16 MLs of InP deposition on a GaAs substrate. We find that after the deposition of approximately 4 MLs of InP, island growth occurs. Islands have sloping <113> sides oriented along the [1$\underline{1}$0] direction and are starting to merge after the deposition of approximately 16 MLs. The effects of substrate temperature are also being studied.

4. Laser induced fluorescence

This section describes the methods used to obtain chemical species identification, concentration and reaction rates by in-situ LIF during a GSMBE growth run. The first important task is to measure the sticking coefficient of various group III elements and group V dimers in the GSMBE system by LIF. Experimentally the determination of the group III atom sticking coefficient is much easier than for those of group V dimeric species. The following describes some basic results that we have obtained in monitoring the group V dimeric P_2 species and its concentration dependence versus temperature above an InP surface.

When LIF is used to measure flux intensity in an MBE chamber, both incident and reflected fluxes are measured because of the Knudsen cell and substrate holder geometry. The total flux measurement can easily be corrected for the offset of the incident flux and the time dependent reflected flux intensity can thus be obtained.

Since the substrate surface is at a constant temperature, the signal we monitor after the incident flux goes to zero (ie the MBE shutter is closed) is the isothermal desorption flux [25]. From this measurement , the desorption rate can be measured for the 100% coverage case and the correction for the sticking coefficient can be obtained.

Assuming a first order desorption, the desorption rate follows an Arrhenius behavior:

$$k = v \exp\left(\frac{-E}{k_B T}\right)$$

where T is the substrate temperature, E is the energy barrier for the desorption, and v is the pre-exponential factor, which does not have as clear a physical interpretation as the one in gas phase. The energy barrier for desorption can thus be derived from the temperature dependent measurements of the desorption rate. This is applied to both the diatomic group V species obtained from pyrolizing AsH_3 and PH_3 and then to the atomic indium species produced by thermal effusion cells.

4.1. Group V species

For the group V dimer flux, the measurements of sticking coefficient and desorption rate are more complicated than the group III element flux because of the molecular energy distribution among the many vibrational and rotational states. Fortunately, the internal energy stored in the vibrational and rotational states can also be quantified by LIF. Since LIF has the capability to monitor the dimer flux intensity for a particular rotational and vibrational state, we can in principle, measure the sticking coefficient and the desorption rate of different vibrational and rotational states. Any possible internal energy dependence of surface growth kinetics can thus be studied.

Initial experiments we performed investigated the thermal desorption of P_2 from the InP surface. The P_2 C-X(1,0) LIF spectrum and the calculated spectrum are shown in the top and bottom parts of figure 13, respectively. The calculated spectrum used the molecular constants given by Herzberg. There is good agreement in the position of the transitions between theory and experiment, indicating that the chemical species P_2 has been identified. The extra lines and energy level shift in the high J states are due to the perturbation of the C state by the nearby c state in a low J state. At low J states both line positions and intensities fit well with the calculations indicating a smaller perturbation. Also observed is that the P and R branch transitions are well separated. Because the C(v=1) state is not perturbed by the nearby c state, we can use the C(v=1) state to monitor the ground state population during MBE growth. This is the procedure that we use.

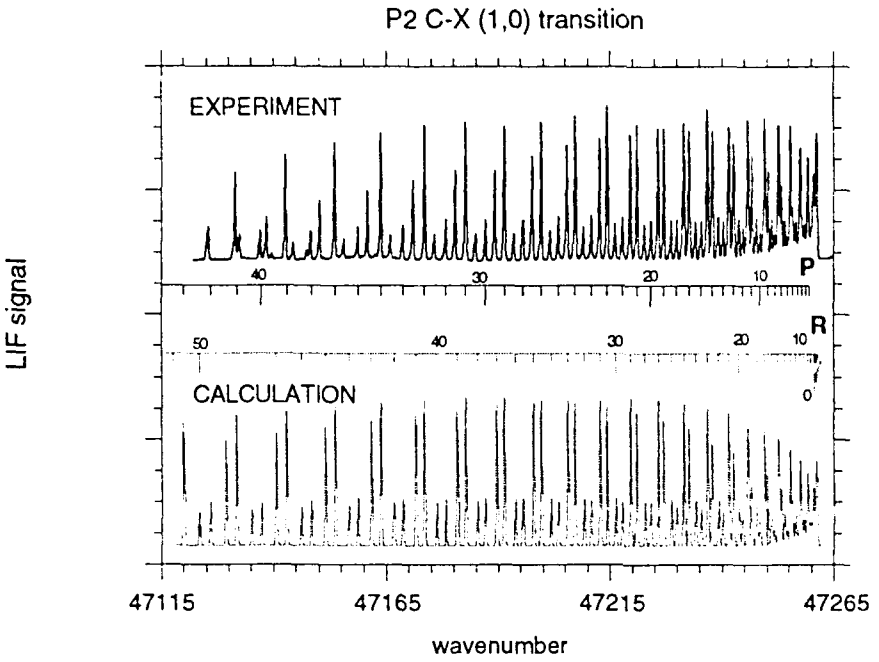

Figure 13 Measured (top) laser induced fluorescence spectrum of P_2 molecules desorbing from an InP substrate. The bottom curve is a simulated spectrum of the P_2 C-X(1,0) transition. Comparison of the two confirms that the desorbing species is actually P_2.

The P_2 C-X(2,0) transition is used to monitor the temperature dependence of P_2 desorption from the InP substrate. As shown in figure 14, there is a strong dependence of LIF intensity as a function of substrate temperature. The relative P_2 partial pressure is measured by integration of the first six peaks of the P_2 LIF spectrum. Because the vibrational and rotational state Boltzmann distributions are the same for the range of temperatures considered, the integral is directly proportional to the P_2 desorption rate. By normalizing the area to the measured 833K value, we obtain the relative P_2 pressure at different substrate temperatures.

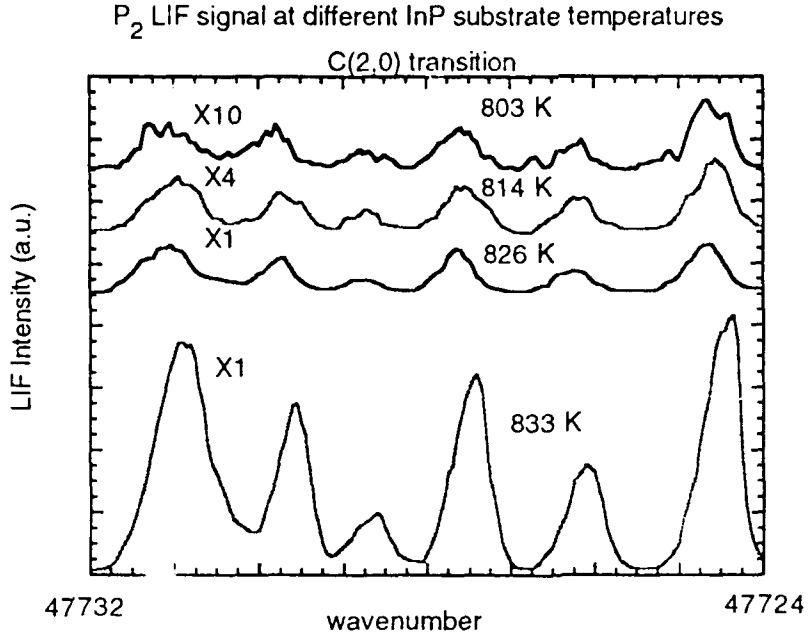

Figure 14 First six peaks of the P_2 C(2,0) transition as a function of temperature showing the thermal decomposition of an InP substrate. The integrated LIF signal is proportional to the partial pressure of the dimeric species.

The temperature dependent pressure from P_2 desorption can then be described by the simple equation

$\ln(P) = -A/T + B$

as shown in figure 15. The measured pressure has the expected exponential temperature dependence.

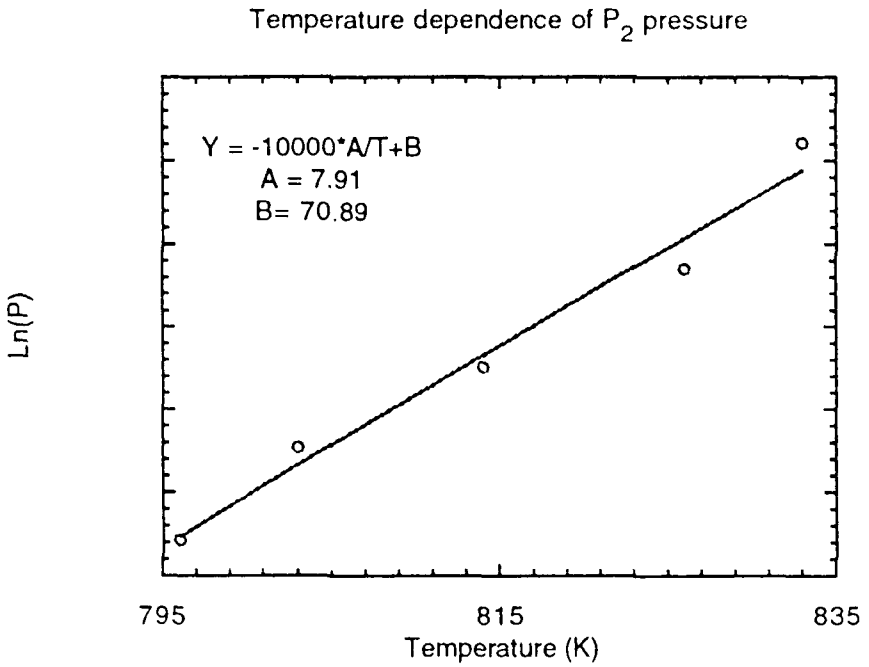

Figure 15 Plot of the logarithm of P_2 pressure versus temperature taken from the LIF spectra. The exponential behavior is clearly indicated from the linear fit.

Monitoring of the LIF spectra of group III atoms is simpler because of the significantly smaller vibrational and rotational states. We have successfully monitored Ga and In using the LIF technique. An advantage of LIF over modulated beam mass spectrometry (MBMS) in measuring group III concentrations is that the LIF technique lends itself to spatial probing of chemical species away from the growth surface thus facilitating the determination of absolute concentrations of incident and desorbing species.

4.2. Group III species

In the present experiment, we monitored the atomic or molecular state population 0.5 cm above the MBE growth surface. We also monitored the internal state population before and after the reaction to understand effects of the excess internal energy in the gas and solid surface reaction.

The desorption of the atomic indium signal was monitored by LIF using the energy level scheme shown in Figure 16.

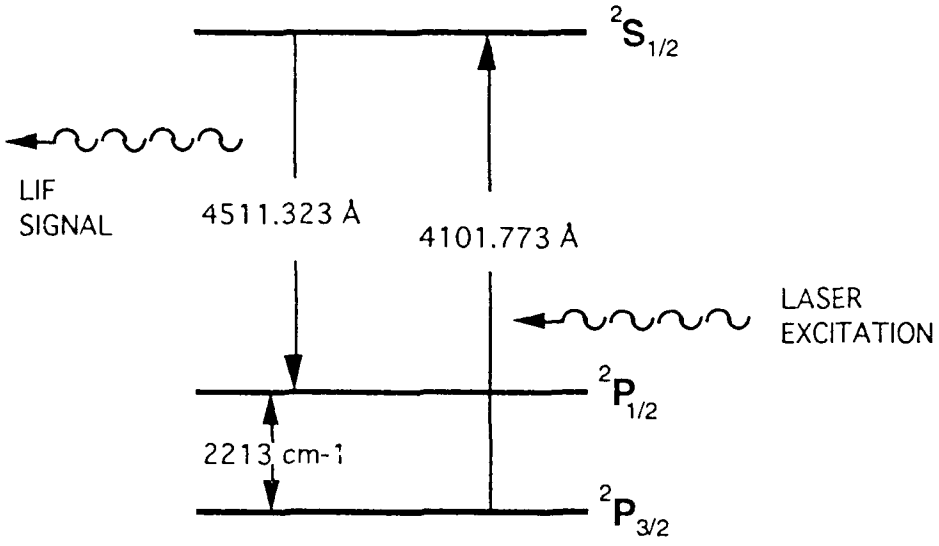

Figure 16. Indium atomic energy level configuration used in the LIF experiment. The In atom $^2S_{1/2}$- $^2P_{3/2}$ transition is excited by a tunable excimer dye laser at a wavelength of 4101.3 Å. The excited state population is monitored by the $^2S_{1/2}$- $^2P_{1/2}$ LIF signal at 4511.3 Å.

Radiation of wavelength 4101.7 Å is used to excite the indium spin-orbit ground state atoms. The 4101.7 Å photon is generated from a LUMONICS HYPER-DYE 300 dye laser pumped by a LUMONICS EX-520 excimer laser. QUI dye is used to obtain an output power of ~1mJ/pulse at 4101.7Å with a 10 ns pulsewidth. The diameter of the dye laser beam is about 2×4 mm before entering the UHV chamber. The laser beam is parallel to the substrate surface and is about 0.5 cm above the surface.

The spin-orbit splitting of the indium atom ground state is more than 2000 cm^{-1}. By assuming a 900°C Boltzmann distribution, we estimated that 95% of the In atoms from the effusion cell should be in the ground spin-orbit state. The fluorescence signal of both 4101.7 and 4511.3 Å can be used to monitor the population of indium atoms in their ground spin-orbit state and excited spin-orbit state. To prevent optical saturation effects the dye laser power is reduced to 10μJ/pulse or less by neutral density filters.

We also monitored the indium spin-orbit excited state desorption from the surface by tuning the dye laser output wavelength to 4511.3Å. The 4101.7Å LIF signal was collected from the PMT by using narrow band bandpass filter centered at 4100Å to filter out scattered light from the dye laser output. Using this technique, the DAE for both indium spin-orbit states which are separated by 0.27 eV can be measured. This is a improvement over the quadrupole mass spectrometry (QMS) and any RHEED type of surface coverage measurement apparatus which can not distinguish the internal excitation of desorbing indium atom.

4.2.1. Indium desorption from homoepitaxial layer by temperature programmed desorption(TPD)

TPD [26] has been used to measure the group III activation energy in the thermal desorption experiment. The thermal desorption rate, R, can be described as

$$R = A\,\theta^n\, e^{-E/kT} \qquad (1)$$

where A is the frequency factor, θ is coverage, n is the order of kinetic process, k is Boltzmann constant, T is the substrate temperature (K), and E is the DAE. For a linear heating rate of the substrate, T can be expressed as

$$T = T_O + \beta t \qquad (2)$$

where T_o(K) is the initial temperature, β is the heating rate(K/sec.), and t is the time(second).

In order to study the In DAE from the homoepitaxial layer, a thick (approximately 0.7μm) layer of InAs is grown on a GaAs substrate. These thick layers of InAs growth on GaAs well exceeds the critical thickness for dislocation formation, thus the strain force between InAs and GaAs due to the large difference between their lattice constant is relaxed in these layers. The complete relaxation of InAs on GaAs can be obtained after the growth of 0.7μm of InAs [27]. The thick InAs layer has complete coverage on the surface and undergoes a first order desorption process in our TPD experiment due to the 2D growth of InAs [28, 29]. The measured activation energy should thus be dominated by the indium bonds with the nearby indium and arsenic atoms. The bond energies are determined by the reconstructed surface of the desorbing surface which is a function of surface temperature.

Three different types of reconstructed InAs surfaces have been observed by RHEED. The As-stabilized surface corresponds to a 2×4 RHEED pattern at lower substrate temperatures(for substrate temperature below 495 °C) compared to a 4×2 RHEED pattern at higher temperatures(495 °C to 545 °C) for an In-stabilized surface. The phase change from an As-stabilized to an In-stabilized surface is extremely sharp(495 °C) and occurs without hysteresis in temperature as described by Schaffer et al. [27]. This phase transition temperature depends on the arsenic flux. A consistent arsenic flux dependent phase transition temperature compared to Schaffer's [27] result has been observed from our GSMBE. We monitor the RHEED pattern to determine the surface reconstruction and correlate with the DAE measurement to determine the surface structure at different surface reconstructions.

We observed that the desorption LIF signal is very dependent on the initial state of the surface. The substrate temperature can be increased to change from an As-stabilized surface to an In-stabilized surface. When the temperature is again lowered, the As-stabilized condition is again observed. This shows that the InAs layer is at the same 2D epitaxy condition and that irreversible arsenic depletion does not occur during our TPD experiment.

Shown in figure 17(a) and 17(b) are desorption signals corresponding to 1.5 ML and 0.7μm of InAs in the In-accumulated regions measured by LIF.

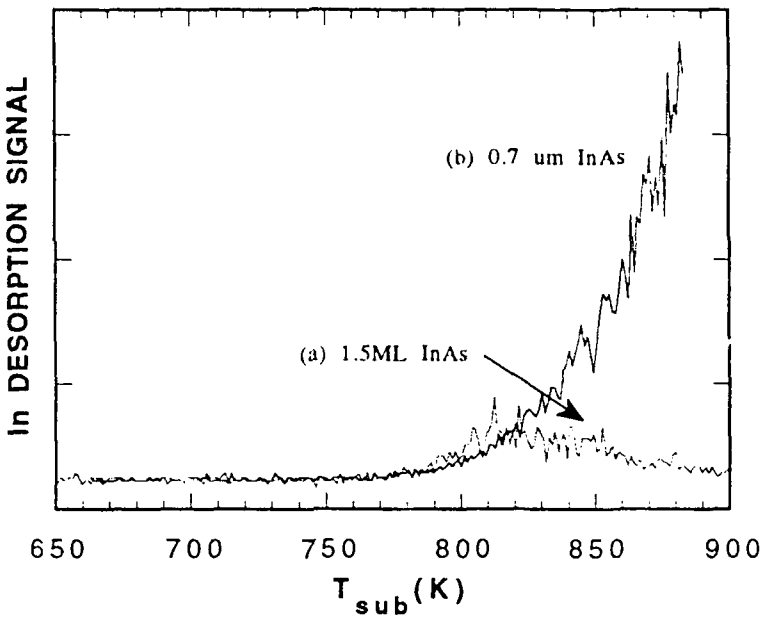

Figure 17 Indium atom TPD desorption signal a) for 1.5 ML coverage of InAs and b) for 0.7 μm thick InAs layer (2D growth).

The decreasing desorption signal of curve 17(a) at higher temperatures is an indication the depletion of the InAs epitaxial layers on the GaAs substrate. The steady exponential increase in desorption signal in Figure 17(b) is a clear indication of constant coverage, (θ=1 in this experiment), throughout the entire TPD process. The observed LIF indium atomic signal in the TPD experiment can be directly correlated to the temperature dependent desorption rate R given in eq. 1.

Since the LIF signal is a direct measurement of the temperature dependent desorption rate, the DAE can be derived from Eq. 1 to be:

$$\ln(\text{indium signal}) = \ln(A) + (-E/kT). \qquad (3)$$

By plotting natural log of indium signal vs. 1/T, this slope should correspond to -E/k. The relative temperature dependent desorption rate data at different reconstructed InAs surfaces are shown in Figure 18.

The arsenic flux remained on during the TPD experiment to prevent the arsenic depletion from the InAs layer and to maintain the same surface reconstruction during the substrate temperature ramp. The different DAE at surfaces with different reconstruction are obtained by changing the range of temperature ramp. Reconstructions are monitored by the RHEED to verify the surface condition.

The DAE values are calculated from a linear least squares fit to be E_{act} = 3.12 ± 0.07 eV for the As-stabilized condition, E_{act} = 3.14 ± 0.12 eV for In-stabilized condition and E_{act} = 2.49 ± 0.04 eV for In-accumulated condition (see Figure 18(c), (b) and (a)). There is no difference in measured DAE between In-stabilized and As-stabilized surface. The indium spin-orbit excited state DAE was measured under In-stabilized conditions to be E_{act} = 3.18 ±

0.10 eV (see Figure 18(d)). The DAE measured from monitoring of indium spin-orbit ground and excited states were the same.

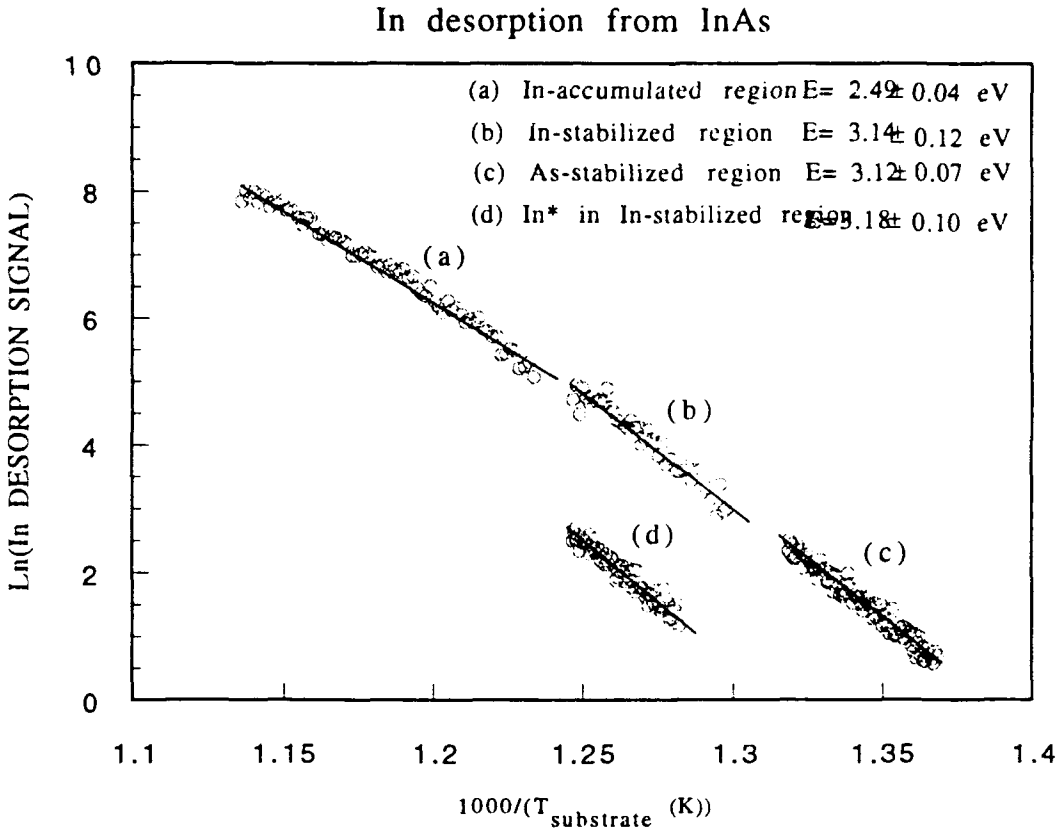

Figure 18 Arrhenius plot of Ln(In desorption signal) vs. $1000/T_{substrate}$. The curves are a) TPD signal from InAs 2D layer in In-accumulated condition with $E_{act.} = 2.49 \pm 0.04$ eV; b) TPD signal from InAs 2D layer in In-stabilized condition with $E_{act.} = 3.14 \pm 0.12$ eV; c) TPD signal from InAs 2D layer in As-stabilized condition with $E_{act} = 3.12 \pm 0.07$ eV; d) TPD signal from InAs 2D layer in In-stabilized condition by monitoring indium spin-orbit excited state desorption with $E_{act} = 3.18 \pm 0.10$ eV

Figure 18 can be explained by considering the reconstructed surface. The As-stabilized InAs surface reconstruction is not known, however the information from the As-stabilized GaAs surface can be applied to InAs. The As-stabilized reconstructed surface of GaAs has been reported by Chadi [30, 31] and the image of this surface has been observed by Pashley et al. [32] and Biegelsen et al. [33] by using scanning tunneling microscopy(STM). The As-stabilized surface from STM image is believed to be the missing dimer and arsenic dimer model as shown in Figure 19(a). The normal temperature range for As-stabilized conditions in our TPD experiment is constrained by the detectability of the indium LIF signal. In our TPD experiment the 2×4 As surface coverage should be 50% [33] as shown in Figure 19(b) instead of 75% [32] as shown in Figure 19(a). No model has been proposed for the Ga-stabilized surface. The reconstructions in Figure 19(c) and Figure 19(d) are possible for the In-stabilized surface from the standpoint of the observed 4×2 RHEED pattern.

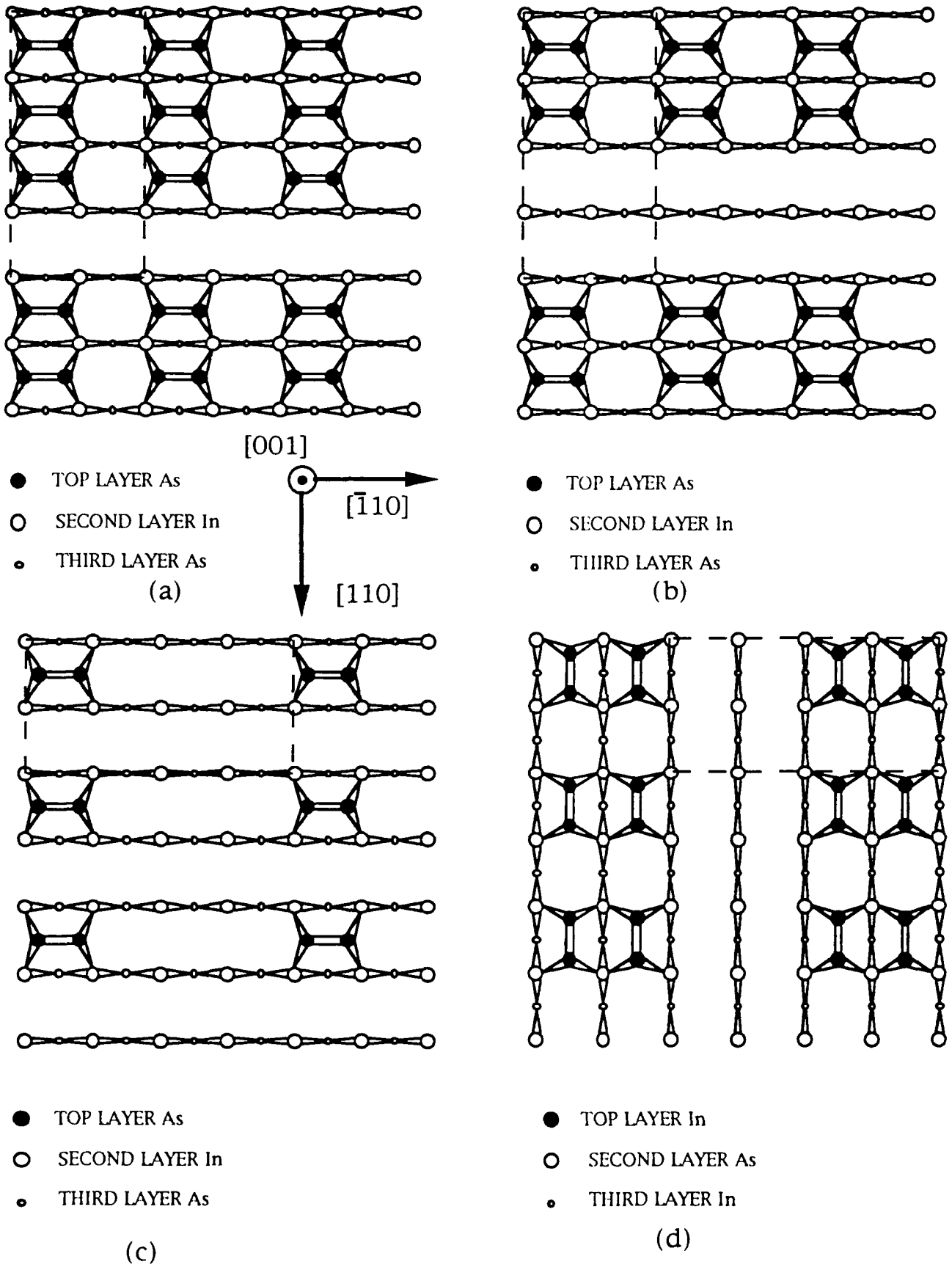

Figure 19 Schematic representation of the InAs surface at different reconstructions; (a) 75% arsenic coverage at As-stabilized surface [34]; (b) 50% arsenic coverage at As-stabilized surface [32,33]; (c) 25% arsenic coverage at In-stabilized surface proposed by the

present study; (d) Initial stage of indium dimerization in In-accumulated region proposed by the present study.

Since the same DAE was observed for the InAs in As-stabilized and In-stabilized conditions, we could argue which of Figure 19(c) or Figure 19(d) is the possible reconstructed surface. Because the In-stabilized reconstructed surface in Figure 5(d) has indium dimer pairs on the surface, we could conclude that the indium DAE in In-stabilized condition should be much lower than on the As-stabilized surface due to the lower bond energy of indium dimers. We should also observe an indium desorption signal equivalent of 0.5 ML from the sharp phase transition of As-stabilized surface to In-stabilized surface. No abrupt change of the indium desorption signal was observed in our TPD experiment. This leads to the conclusion that Figure 19(d) is not the In-stabilized surface for InAs homoepitaxial layer. We could argue the 25% As coverage as shown in Figure 17(c) is the possible surface structure. For InAs in As-stabilized conditions, by considering only the interaction with the first two zones of nearby atoms, each indium is surrounded by two first nearest neighbor arsenic atoms and four second nearest neighbor indium atoms. The difference between the In-stabilized and As-stabilized surfaces per unit cell is that the indium atom in the As-stabilized surface is bounded by two more nearby arsenic atoms from the arsenic dimer pair. The DAE experiment measures the statistical average of the indium bond energy at different indium locations as shown in Figure 19(b) and 19(c). The difference between these two could be too small to be resolved by the TPD measurement.

The other possible explanation for same DAE on both In-stabilized and As-stabilized surfaces is that the indium binding force changes at the time it desorbs from the surface. Since the InAs congruent sublimation temperature is only 380 °C, the arsenic dimer pairs does not stay on the surface permanently. Arsenic dimer pairs are formed and broken on the InAs surface throughout the TPD experiment. The indium desorption that we measure is during the time that As dimer pairs are missing from the surface. Since the RHEED pattern is the time averaged measurement of the diffraction pattern, the 2×4 and 4×2 RHEED pattern for the As-stabilized and In-stabilized surfaces are still observed instead of 1×1 RHEED pattern. During the time of indium desorption, indium atoms only feel the binding force from two first nearest neighbor arsenic atoms and four second nearest neighbor indium atoms in either As-stabilized or In-stabilized surfaces. This could be another explanation for observing the same DAE for both In-stabilized and As-stabilized surfaces.

When the surface reached the In accumulated condition, which occurred at a higher substrate temperature(≥550 °C) than for the In-stabilized condition, the observed 4×2 structure could result from the indium dimerization on the surface. This could explain the DAE measurement in In-accumulated region was 0.6 eV lower than the observed indium DAE in In-stabilized and As-stabilized surfaces. The RHEED pattern still remained 4×2 during the change from an In-stabilized to In-accumulated surface. The surface structure during the temperature ramping from our TPD experiment suggests the sequence of Figure 19(b), Figure 19(c) and Figure 19(d). At surface temperatures higher than those for In-stabilized conditions, the In coverage would change from 50% to 75% and eventually the surface would be covered with indium atoms. This caused a complete depletion of As from the InAs layer which prohibited the recovery of the InAs surface. The smooth change of arsenic to indium coverage on the surface from Figure 19 gives the best interpretation of how the surface coverage changes at different reconstructed surface so far.

The other interesting result is that no difference is observed in the DAE from monitoring indium spin-orbit ground and spin-orbit excited states. If the bond breaking of the indium on the InAs also included the internal excitation of the desorbing indium, we should

expect the indium spin-orbit excited state should have a DAE 0.27 eV higher than DAE from spin-orbit ground state. The reason for no difference in our observation for excited state is due to the slow heating of the substrate in the TPD experiment. In the slow heating during thermal desorption process, the indium internal excitation is characterized by the Boltzmann distribution. The ratio of LIF signal for indium excited state to indium ground state is 1:40 which is similar to the calculation of LIF signal from the Boltzmann distribution and transition dipole moment. The phase space theory modeling of internal excitation by one photon laser excitation in the gas phase photo dissociation process [34] can not be applied in the TPD experiment.

4.2.2. Indium desorption from submonolayers of InAs on GaAs

Indium desorption from submonolayers can provide information of heteroepitaxial growth during the initial growth stages. Although the TPD can not observe the growth mode during the growth process, the desorption kinetic order after growth can be determined from TPD. The differences in the kinetic order during TPD can be used to determine the growth mode in the early stages of heteroepitaxial growth [25].

The submonolayer deposition of InAs on the GaAs (001) surface is achieved by reducing the In cell temperature from 870 °C to 700 °C. The InAs growth rate at 700 °C was approximately 0.02ML/sec as observed by RHEED oscillations. The GaAs substrate temperature and arsenic flux remained constant during the ITD experiment. The arsenic flux was used mainly to maintain the GaAs surface under an As-stabilized condition which was confirmed by observing a 2×4 RHEED pattern.

The LIF signal for the ITD on InAs from GaAs is shown in Figure 20. Region I corresponds to the indium LIF signal before indium deposition which is the measurement of the growth chamber indium background signal (shutter off). Region II corresponds to the indium LIF signal during the indium deposition which lasted about 30 second(shutter open), and region III corresponds to indium LIF signal after the deposition was stopped(shutter closed). The LIF signal in region II is the sum of incident indium flux(J_o), indium desorption from indium deposited on GaAs substrate, and indium deflected from the GaAs surface due to the sticking coefficient not being equal to 1 at each particular substrate temperature. The indium LIF signal in region III is only due to the ITD of a submonolayer of indium from GaAs surface.

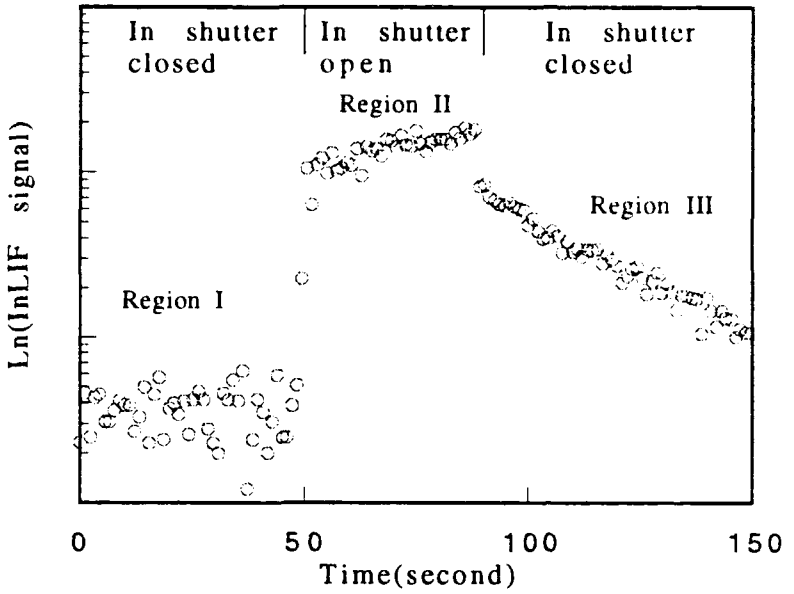

Figure 20 Natural log plot of indium LIF signal in ITD experiment vs. time. Region I is indium LIF signal with the indium shutter closed before deposition, region II is the indium LIF signal with indium shutter open during the deposition, and region III is the indium LIF signal with indium shutter closed after the submonolayer indium was grown.

The change of LIF signal in regions II and III can be expressed as follows:

$$\frac{d\theta}{dt} = J_o\ S\ (1-\theta(t))-A\theta(t)e^{-E/kT} \qquad (4)$$

where S is group III(indium) sticking coefficient, J_o is the incident indium flux, and the rest of the symbols are the same as in Eq. 1. The first term in Eq. 4 describes the change of indium coverage on GaAs surface due to the incident indium flux, and the second term in Eq. 4 represents the change of the indium coverage due to ITD. The choice of the first order kinetic for thermal desorption is clear from the data in Figure 20. Since the ITD signal in region III can be fitted by a single exponential decay curve, this should correspond to first order desorption kinetics. The observed indium LIF signal in region II can be described as follows:

$$J_o+J_oS\theta(t)+A\theta(t)e^{-E/kT} \qquad (5)$$

where $\theta(t)=\frac{J_oS}{J_oS+Ae^{-E/kT}}\ (1-e^{-tB})$ and $B=e^{-(J_o\ S\ +\ A\ e^{-E/kT})}$. The observed indium LIF signal in region III can be described as follows:

$$Ae^{-E/kT}\ \theta_o\ e^{-Ate^{-E/kT}} \qquad (6)$$

where θ_o is the indium coverage at the end of indium deposition.

The expression in Eq. 5 shows that the LIF signal should reach an asymptotic value after $\theta(t)$ reach it's asymptotic value due to the balance between indium adsorption and

desorption on the GaAs surface. This can be used as the baseline value. By subtracting the LIF signal value by this value we should be able to obtain the DAE for submonolayer indium desorbed from GaAs. Since the indium deposition time is not long enough in the present study to obtain the plateau in the indium LIF signal, we will use this as a tool for independent confirmation for future submonolayer desorption studies.

From Eq.6 it is clear the slope of Ln(In LIF signal) v.s. time should give us the value of $Ae^{-E/kT}$ from our ITD curve as shown in Figure 20. This value is a function of substrate temperatures. By plotting $Ln(Ae^{-E/kT})$ vs. 1/T, the slope should give us the submonolayer indium DAE from the GaAs surface, and the intercept at 1/T=0 should give us the value of preexponential factor called the desorption frequency factor [31].

The indium desorption rate temperature dependence from submonolayer indium on GaAs is shown in Figure 21.

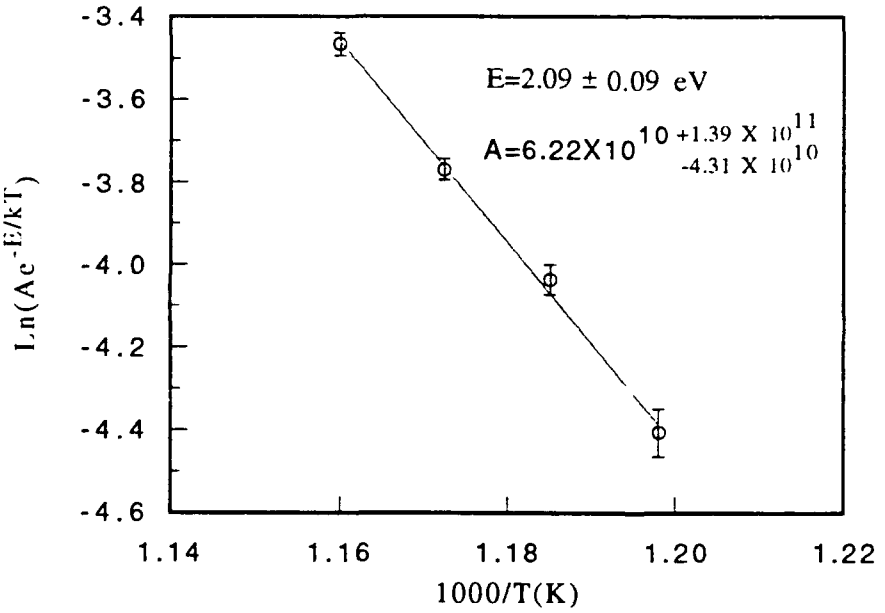

Figure 21 Arrhenius plot of $Ln(Ae^{-E/kT})$ vs. 1000/T(K). The DAE from the submonolayer InAs on GaAs is estimated to be 2.09 ± 0.09 eV, and the preexponential factor is measured to be $6.22\times10^{10\ +1.39\times10^{11}}_{\ -4.31\times10^{10}}$ s^{-1}.

The DAE measured from the present experiment is 2.09 ± 0.09 eV. This value is in good agreement with the early total reflection angle X-ray spectroscopy in RHEED(RHEED-TRAXS) by Shigetomi [35] et al. In their ITD experiment, the surface coverage of indium was measured instead of desorption rate from our LIF experiment. The measured submonolayer indium desorption energy from their experiment is 2.1 eV. Two different experimental techniques give the same indium submonolayer DAE energy within the experimental error. The preexponential factor from our experiment has been estimated to be $6.22\times10^{10\ +1.39\times10^{11}}_{\ -4.31\times10^{10}}$ s^{-1} which is in good agreement with the theoretical value by Kern et al. [29] which should be in the range of 10^{11} to 10^{15} s^{-1}. The agreement in the value of the

preexponential factor also confirms that the order of desorption kinetics should be equal to 1. 3D indium nucleation is not present at the low indium coverages in our present study.

In summary, the technique of LIF with TPD and ITD is proved to be a viable technique to investigate the growth kinetics in MBE [36]. We can measure not only the DAE, we can also determine the desorption kinetics order for the heteroepitaxial layer. The In-stabilized InAs surface is believed to be 25% arsenic coverage as shown in Fig 19(c). From Eq.5, the sticking coefficient of indium on submonolayer indium coverage on GaAs can be obtained. This work has set the basis for future studies on this topic.

5. Summary

We have demonstrated a multifaceted approach to measuring growth processes in solid and gas source MBE. This includes the development and implementation of in-situ growth monitoring techniques that characterize optical, chemical and structural properties of the growing epitaxial layers. Our laboratory is unique in that these analyses can be combined to produce information for growth models. Using these methods, we have obtained record quantum well PL linewidths, observed interface smoothing at heterojunctions by ellipsometry, identified the atomic and dimeric chemical species above the growing surface, extended the range of substrate temperature determination from 400°C down to room temperature and tracked the growth of quantum wells by optical techniques. Additionally it has enabled us to realize microcavity Fabry-Perot electro-optic modulators with record performance. The information obtained will be used by our group and others to model the growth of semiconductor materials and heterojunction interfaces.

6. References

[1] K.T. Shiralagi, K.Y. Choi, R. Droopad, G.N. Maracas, "Hydride Cracker Nozzle Design for Gas Source Molecular Beam Epitaxy," submitted to J. Vac. Sci. Tech. March 1991.

[2] G.N. Maracas, J.L. Edwards, K. Shiralagi, K.Y. Choi, R. Droopad, B. Johs and J.A. Woolam, J. Vac. Sci. Tech. A 10(4) (1992)

[3] D. E. Aspnes, Thin Solid Films, 89 (1982) 249

[4] D. E. Aspnes, W. E. Quinn, S. Gregory, Appl. Phys. Lett. 56 (1990) 2569

[5] B. Johs, J.L. Edwards, K.T. Shiralagi, R. Droopad, K.Y. Choi, G.N. Maracas, D. Meyer, G. Cooney and J.A. Woolam, Materials Research Society, Spring 1991 Meeting, Anaheim, CA

[6] D. E. Aspnes in Optical Properties of Solids: New Developments, edited by B. O. Seraphin (North-Holland, Amsterdam, 1976), p. 799.

[7] H. Yao, P G. Synder, and J. A. Woollam, J. Appl. Phys., 70(6), 3261 (1991)

[8] M. M. Ibrahim and N. M. Bashara, J. Vac. Sci. Technol. **9**, 1259 (1972).

[9] Takishi Tomita, Toshiaki Kinosada, Tatuya Yamashita, Masahio Shiota and Takeshi Sakurai, Jap. JAP **25**, L925 (1986).

[10] J. L. Edwards, K.Shiralagi, K. Y. Choi, R. Droopad, G. N. Maracas, B. Johs and J. A. Woollam, submitted to Applied Physics Letters

[11] M. Garriga, P. Lautenschlager, M. Cardona and K. Ploog, Solid State Communications, 61, 157, (1987)

[12] E.D. Palik in Handbook of Optical Constants of Solids II, pp. 489-499, Academic Press, San Diego, (1991)

[13] G.N. Maracas and J.L. Edwards, to be published

[14] D.E. Aspnes, W.E. Quinn and S. Gregory, Appl. Phys. Lett. **56** (25), pp.2569-2571, 1990

[15] J.L. Edwards, K.T. Shiralagi, K.Y. Choi, R. Droopad and G.N. Maracas, "In-situ and Ex-situ Characterization of GaAs/AlAs Quantum Well Structures Using Spectroscopic Ellipsometry," Third International Conference on Chemical Beam Epitaxy, Oxford, UK, (1991)

[16] J.L. Edwards, G.N. Maracas, K.T. Shiralagi, K.Y. Choi and R. Droopad, "In-situ and ex-situ characterization of Gas/AlAs quantum well srtuctures using spectroscopic ellipsometry," J. Cryst. Growth 120, pp78-83 (1992)

[17] J.D. Walker, K. Malloy, S. Wang and J.G. Smith, Appl. Phys. Lett. 56(25), 2943-2495 (1990)

[18] R.M.A. Azzam and N.M. Bashara, Ellipsometry and Polarized Light, 288-315, North Holland/Elsevier, New York (1987).

[19] K.T. Shiralagi, R.A. Puechner, K.Y. Choi, R. Droopad, and G.N. Maracas, to appear in J. Cryst. Growth, August (1991)

[20] D. Saluja, P.R. Pukite, S. Batra and P.I. Cohen, "RHEED measurements of AlGaAs grown instabilities and roughening rates on misoriented substrates," J. Vac. Sci. Tech., **B5**(3), pp. 710-713 (1987).

[21] P.R. Pukite, J.M. Van Hove and P.I. Cohen, "Extrinsic effects in high-energy electron diffraction patterns from MBE GaAs," J. Vac. Sci. Tech., **B2**(2), pp. 243-248 (1984).

[22] J.M. Van Hove and P.I. Cohen, "Development of steps on GaAs during MBE," J. Vac. Sci. Tech., **20**(3), pp. 726-729 (1982).

[23] K.T. Shiralagi, R.A. Puechner, K.Y. Choi, R. Droopad, and G.N. Maracas, to appear in J. Cryst. Growth, August (1991)

[24] K. Shiralagi, A. Kriman, R. Droopad and G.N. Maracas, "Effusion Cell Orientation Dependence of MBE Flux Uniformity," J. Vac. Sci. Tech., A 9(1), pp. 65-70, (1991)

[25] R. V. Smilgys and S.R. Leone, J. Vac. Sci. Technol. **B8**, 416 (1990).

[26] P. A. Redhead, Vacuum **12**, 203 (1962).

[27] W. J. Schaffer, M.D. Lind, S.P. Kowalczyk, and R.W. Grant, J. Vac. Sci. Technol **B 1**, 688 (1983).
[28] L.A. Petermann, Progress in Surf. Sci. **3**, 1 (1972).
[29] *Current Topics in Materials Science*, Vol 3, Ed. by E. Kaldis (North-Holland Publishing Company, 1979).
[30] D.J. Chadi, J. Vac. Sci. Technol **A 5**, 834 (1987).
[31] P.K. Larsen and D.J. Chadi, Phys. Rev. **B 37**, 8282 (1988).
[32] M.D. Pashley, K.W. Haberern, W. Friday, J.M. Woodall, and P.D. Kirchner, Phys. Rev. Lett. **60**, 2176 (1988).
[33] D.K. Biegelsen, R. D. Bringans, J.E. Northrup, and L.-E. Swartz, Phy. Rev. **B41,** 5701 (1990).
[34] Hyun-Sook Kim, Chau-Hong Kuo, and Michael T. Bowers, J. Chem. Phys. **93**, 5594 (1990).
[35] J. Shigetomi, K. Fuwa, S. Shimizu, and H. Yamakawa, J. Crystal Growth **111**, 110 (1991).
[36] Chau-Hong Kuo, Calvin Choi, and George N. Maracas, Timothy C. Steimle, "Measurement of Indium Desorption Activation Energy from InP Layers by Laser Induced Fluorescence," submitted to J. Cryst. Growth 8/92

7. Figure Captions

Figure 1 A comparison of substrate temperature determined by thermocouple, optical pyrometer and spectroscopic ellipsometer. The difference between the thermocouple and ellipsometer is plotted on the axes to the right. It should be noted that the ellipsometer can measure temperature from typical growth temperatures to room temperature.

Figure 2 Dynamic fitting of Δ versus time during the growth of AlAs. The growth rate of 0.77 ML/s was extracted by the dynamic fit over approximnately 15 minutes of data.

Figure 3 Real-time monitoring by of the growth of a thick (2500Å) AlGaAs epitaxial layer on a GaAs substrate. This curve was taken at a wavelength of 5000Å.

Figure 4 The velocity plot corresponding to the growth run shown in figure 2 shows the spiraling of the trajectory to the optically thick values of GaAs and AlGaAs at the wavelength of 5000Å.

Figure 5 Tracking of two quantum well growth runs. One quantum well had a 60 second interruption at the "inverted" GaAs on AlAs surface while the other had none.

Figure 6 Raw data for SE scan of the two AlAs/GaAs quantum well structures (one with interruption and the other without growth interruption at the "inverted" interface).

Figure 7. Dynamic growth monitoring of a 20 period AlAs/AlGaAs distributed Bragg reflector in the MBE at the growth temperature of 623°C. The periodicity of the mirror is evident in Ψ as a function of time. Superimposed are the curves of periods 1, 2-5, 6-10, 11-15 and 16-20 identified when the periods end. The time axis has been shifted such that successive period scans begin at t=0. A high degree of thickness and alloy composition reproducibility is evident from the superimposed curves.

Figure 8. Measurement of Ψ versus wavelength of a distributed Bragg reflector at the growth temperature of 623°C in the MBE. The spectra were taken before the epitaxial structure was grown and after the growth of 1, 5, 10, 15 and 20 periods of the mirror. The angle of incidence of the incident light was 75°.

Figure 9. Normal incidence reflectance of a 20 period AlAs/AlGaAs distributed Bragg reflector. The mirror was designed for λ=867nm. The as-grown structure parameters were measured by SE at 623°C. Measured and calculated reflectance curves for the mirror are shown.

Figure 10 Ellipsometric tracking of the growth of a 20 period MBE AlGaAs/GaAs multiple quantum well.

Figure 11 2K PL linewidths are plotted for 50Å, 75Å and 100Å GaAs/ AlGaAs QWs grown at different substrate temperatures. All QWs were grown with only one interrupt at the normal interface except for the QWs grown at 626°C which had interrupts both at the normal and inverted interfaces. The 2K linewidth for the 100Å GSMBE well is 0.62 meV which is close to the best obtained solid source MBE value of 0.5 meV.

Figure 12 The reported best PL linewidths as a function of transition energies for single GaAs/ AlGaAs QWs of different width. Plotted are QWs grown by (●) MOCVD, (+) CBE, (Δ) MBE. Our data for GSMBE growth (■ -solid line) with interrupt at both interfaces and GSMBE (▲ -dotted line) with interrupt at only the normal interface are superimposed.

Figure 13 Measured (top) laser induced fluorescence spectrum of P_2 molecules desorbing from an InP substrate. The bottom curve is a simulated spectrum of the P_2 C-X(1,0) transition. Comparison of the two confirms that the desorbing species is actually P_2.

Figure 14 First six peaks of the P_2 C(2,0) transition as a function of temperature showing the thermal decomposition of an InP substrate. The integrated LIF signal is proportional to the partial pressure of the dimeric species.

Figure 15 Plot of the logarithm of P_2 pressure versus temperature taken from the LIF spectra. The exponential behavior is clearly indicated from the linear fit.

Figure 16 Indium atomic energy level configuration used in the LIF experiment. The In atom $^2S_{1/2}$- $^2P_{3/2}$ transition is excited by a tunable excimer dye laser at a wavelength of 4101.3 Å. The excited state population is monitored by the $^2S_{1/2}$- $^2P_{1/2}$ LIF signal at 4511.3 Å.

Figure 17 Indium atom TPD desorption signal a) for 1.5 ML coverage of InAs and b) for 0.7 μm thick InAs layer (2D growth).

Figure 18 Arrhenius plot of Ln(In desorption signal) vs. $1000/T_{substrate}$. The curves are a) TPD signal from InAs 2D layer in In-accumulated condition with $E_{act.} = 2.49 \pm 0.04$ eV; b) TPD signal from InAs 2D layer in In-stabilized condition with $E_{act.} = 3.14 \pm 0.12$ eV; c) TPD signal from InAs 2D layer in As-stabilized condition with $E_{act} = 3.12 \pm 0.07$ eV; d) TPD signal from InAs 2D layer in In-stabilized condition by monitoring indium spin-orbit excited state desorption with $E_{act} = 3.18 \pm 0.10$ eV

Figure 19 Schematic representation of the InAs surface at different reconstructions; (a) 75% arsenic coverage at As-stabilized surface[15]; (b) 50% arsenic coverage at As-stabilized surface[13,14]; (c) 25% arsenic coverage at In-stabilized surface proposed by the present study; (d) Initial stage of indium dimerization in In-accumulated region proposed by the present study.

Figure 20 Natural log plot of indium LIF signal in ITD experiment vs. time. Region I is indium LIF signal with the indium shutter closed before deposition, region II is the indium LIF signal with indium shutter open during the deposition, and region III is the indium LIF signal with indium shutter closed after the submonolayer indium was grown.

Figure 21 Arrhenius plot of $Ln(Ae^{-E/kT})$ vs. 1000/T(K). The DAE from the submonolayer InAs on GaAs is estimated to be 2.09 ± 0.09 eV, and the preexponential factor is measured as $6.22 \times 10^{10}\ ^{+1.39\times10^{11}}_{-4.31\times10^{10}}$ s^{-1}.